Site-dependent differences in chondrocyte responses to deformation and mechanical properties of rabbit knee joint cartilage

Ari Ronkainen

Master's thesis

Physics training program

University of Eastern Finland, Department of Applied Physics

June 2014

University of Eastern Finland, Faculty of Science and Forestry
Physics training program, medical physics
Ari Ronkainen: Site-dependent differences in chondrocyte responses to deformation and mechanical properties of rabbit knee joint cartilage.
Master's thesis, 80 pages
Supervisors: Post doc researcher, James Fick
Associate Professor, Rami Korhonen
June 2014

Keywords: articular cartilage, chondrocyte, confocal laser scanning microscopy, knee joint, mechanical properties, osteoarthritis

Abstract

Chondrocytes are the cells in articular cartilage (AC) that are responsible for the maintenance of the tissue and remodeling of the extracellular matrix (ECM). ECM molecules, such as collagen and proteoglycan (PG), are synthesized by healthy or normally functioning cells. However, during osteoarthritis (OA), the anabolic and catabolic activity of the chondrocytes is altered, which leads to degeneration of the ECM and changes in the properties of AC. It is known that the mechanical responses of chondrocytes to deformation are also altered during tissue degeneration. However, these studies have been usually performed on a single site or on a few sites of the knee joint. Site-specific responses of chondrocytes to deformation are not known but are important in understanding if and how the mechanical cell responses differ between the various sites within the knee joint. Furthermore, the cell responses to deformation would act as an important control values for future studies.

The primary objective of this research was to investigate site-dependent differences in the mechanical behavior of chondrocytes, by studying the volume and dimensional changes (height, width and depth) of the chondrocytes as a result of tissue loading. Furthermore, global tissue strain, local axial and transverse strains were calculated. In order to study the *in situ* responses of chondrocytes to deformation, a customized indentation device mounted into a confocal laser scanning microscopy was utilized. Samples were harvested from 6 sites in five skeletally mature New Zealand white rabbit knee joints. The sites analyzed included patella, groove and the lateral and medial compartments of both the femoral condyle and tibial plateau. In addition to these cell-level parameters, biomechanical testing was carried out on separate samples to investigate differences in mechanical moduli (equilibrium and dynamic) of cartilage among sites.

Differences were found in chondrocyte mechanical responses across the tissue sites. The differences in volume and dimension changes were consistent with the changes in local axial and transverse strains for the different tissue sites examined. In more detail, for each site the cell volume and height were observed to decrease, while

the cell depth and width increased. The changes due to deformation (mean ± 95% confidence intervals) in cell volumes were smallest in medial condyle tissues ($-6.4 \pm 2.2\%$) and greatest in lateral condyle tissues ($-12.3 \pm 2.1\%$). The smallest changes in cell height, width and depth, were observed in lateral plateau tissues ($-12.5 \pm 1.8\%$, $3.7 \pm 0.9\%$ and $3.5 \pm 1.3\%$; respectively). The greatest changes in cell height and width were observed in medial plateau tissues ($-24.9 \pm 2.8\%$ and $12.4 \pm 1.7\%$; respectively). However, the greatest changes in cell depth were observed in medial condyle tissues ($14.2 \pm 2.0\%$).

Global strains and local axial strains were the smallest in lateral plateau tissues ($9.8 \pm 1.0\%$ and $20.7 \pm 1.5\%$; respectively) and the highest in medial plateau tissues ($22.4 \pm 2.0\%$ and $35.0 \pm 2.3\%$). Overall, global strain values were lower than the local axial strain values, implying that the superficial layers of the tissues were compressed more than the whole tissue. Transverse strains were determined in major and minor directions. The strains in major direction were greatest in medial plateau tissues ($10.9 \pm 1.0\%$) and greatest in minor direction in medial condyle tissues ($6.1 \pm 0.9\%$). The smallest major and minor strains were observed in lateral plateau tissues ($5.1 \pm 0.8\%$ and $2.6 \pm 0.7\%$; respectively). The strain values were consistent with the cell volume and dimensional changes, so that local axial strains caused cell height deformations, and the major and minor transverse strains were causing the width and depth changes, respectively.

The equilibrium and dynamic moduli of cartilage were also different between the tissue sites. The equilibrium moduli were lowest in the patella (0.24 ± 0.06 MPa) and highest in the lateral plateau (0.58 ± 0.08 MPa). The dynamic moduli were lowest in the medial plateau (1.57 ± 0.28 MPa) and highest in the groove (3.58 ± 1.09 MPa). The high equilibrium moduli of the lateral plateau tissues could explain the smaller cell height changes in this site. And vice versa, the low equilibrium moduli of patella tissues could explain the bigger cell height changes in this site. The cell responses, which were measured in equilibrium, can not be straightforwardly compared to the dynamic moduli. However, the high dynamic moduli and low deformation-induced cell volume changes of the groove tissues indicate that this site is one of the stiffer tissue regions in the rabbit knee.

Taken together, the data demonstrates that greater decreases in cell volume were primarily caused by greater decrease in cell height and smaller increases in cell width and depth, which implies that the local ECM structure can prevent cell streching in lateral direction. Also, it seems that mechanical stiffness of tissues is inversely proportional to the cell height changes, which further implies that the tissue structure is driving the mechanical response of chondrocytes. Because chondrocytes can remodel the ECM structure, it is possible that differences between the tissue sites arise from different functional requirements of the joint tissues, which drive the cell biosynthesis and mechanical tissue properties differently in different sites.

Abbreviations

AC	articular cartilage
ACLT	anterior cruciate ligament transection
ADAMTS	a disintegrin and metalloproteinase with thrombospondin motifs
ATP	adenosine triphosphate
AU	arbitrary unit
COX	cyclooxygenase
CS	chondroitin sulfate
DMEM	Dulbecco's modified eagle's medium
ECM	extracellular matrix
GAG	glycoaminoglycan
IF	intermediate filament
IL	interleukin
KS	keratin sulfate
MMP	matrix metalloproteinase
OA	osteoarthritis
PBS	phosphate buffered saline
PCM	pericellular matrix
PG	proteoglycan
TGF	transforming growth factor
TIMP	tissue inhibitor of metalloproteinase

Symbols

$a, b, c, d, e, f, g, h, k$	quadric coefficients
A	area of indenter
$\mathbf{A}$	matrix of partial derivative terms
$\mathbf{b}$	vector of coordinates
C	constant
$\mathbf{D}$	submatrix of quadric coefficients
$\mathbf{E}$	matrix of quadric coefficients
E	Young's modulus
E_{dyn}	dynamic modulus
E_{eq}	equilibrium modulus
$E_{measured}$	Young's modulus from stress-strain curve
E'	storage modulus
E''	loss modulus
E^*	vector sum of storage and loss modulus
F	indentation force
H	tissue thickness
ΔH	change in tissue thickness due to deformation
l_0	distance between unloaded cells
l	distance between loaded cells
L	least squares expression
$\mathbf{P}$	rotated ellipsoid coefficient matrix
r	indenter radius
r_1, r_2, r_3	lengths of ellipsoid semi-principal axes

$\mathbf{R}$	rotation matrix
$\mathbb{R}$	real numbers
t_{tof}	time-of-flight
v_{us}	ultrasound velocity
x, y, z	general coordinates
x_0, y_0, z_0	position of ellipsoid center
$\hat{x}, \hat{y}, \hat{z}$	body coordinates
ϵ	strain
ϵ_{axial}	axial tissue strain
$\epsilon_{\text{transverse}}$	transverse tissue strain
ϵ_{global}	global tissue strain
$[\epsilon]_{2\times2}$	strain tensor
θ	vector of unknowns
κ	scaling factor
$\lambda_1, \lambda_2, \lambda_3$	eigenvalues of $\mathbf{D}$
μ	function of $\mathbf{D}$'s eigenvalues
ν	Poisson's ratio
σ	stress
σ_∞	equilibrium stress
φ	phase lag
ω	angular velocity

Preface

This master thesis was conducted in University of Eastern Finland in Kuopio campus in the Department of Applied Physics and in the Cell and Tissue Biomechanics research group. The aim of this work was to study the mechanical response of chondrocytes to deformation in various sites within a rabbit knee joint.

I would like to thank everyone who participated or contributed to this work in anyway. Especially I want to thank my supervisors post doctoral researcher James Fick and associate professor Rami Korhonen, for their guidance and also for making this project possible. Next, I would like to thank all my friends who helped me to take my thoughts away from the thesis on my free time and help me relax. Also, I would like to thank the Biophysics of Bone and Cartilage research group for an excellent working environment. Last, but definitely not the least, I want to thank my beloved fiancée for all her support during this work.

Kuopio, June 2014

Ari Ronkainen

Contents

Chapter 1

Introduction and aims

Motivation to study synovial joints, e.g. knee or hip joint, arises from the fact that arthritis and other rheumatic conditions are very expensive to the society. In 2003, the United States' annual cost of these diseases was approximately $128 billion [19]. In Finland the annual cost of osteoarthritis (OA), the most common form of arthritis, was approximated to be one billion euros [1]. In OA, the joint surface or articular cartilage (AC) is irreversibly damaged or lost which leads to constricted function of the joint and joint pain [2]. In Finland alone it is estimated that 5 % of men and 7 % of women aged over 30 years old are suffering from knee OA. Corresponding numbers for hip OA are 5 % and 4 %, respectively [1]. In comparison for the U.S. population, it is approximated that 12.1% of the adult population (i.e. 27 million adults) are suffering from some form of OA [3].

OA isn't only a wear and tear type of disease, but instead multiple factors contribute to it [2, 4]. The risk factors of OA include age, obesity, gender, joint injuries, joint deformation and muscle weakness [2, 5–7]. Out of these, aging is the biggest risk factor for OA. Due to this, the prevalence of the disease is rising [3, 7]. In Finland alone more than half of the population aged over 65 and almost 90% of population aged over 75 show joint space narrowing in radiological investigations of the knee, which may indicate alterations in the meniscus and is also usually caused by abnormalities in AC itself, which may suggest the onset of OA [1, 54].

In the first stage of OA, the collagen orientation of the surface layer of AC becomes more random, which can be seen as articular surface fibrillation [15]. This

destruction of the collagen network causes proteoglycan (PG) loss in the extracellular matrix (ECM) and tissue swelling [15, 16]. These changes cause signalling cascades, that lead to cell division and increased synthetic activity of chondrocytes [50]. However, the relatively slow division of the chondrocytes and synthesis of ECM molecules is overcome by extensive damage to the ECM, if abnormal joint loading or joint injury is prolonged [50, 55]. Hence, the chondrocytes' response to the mechanical environment plays an important role in the progression of OA [55].

Altered biomechanics may lead to changes in cell biosynthesis during OA, but the cell responses to mechanical loading *in vivo* or *in situ* are not well known in the very early stages of OA [24]. However, it is known that chondrocyte volume and morphology are changing under mechanical stress and during the progression of OA [24, 25]. For example, chondrocyte volume within the superficial and mid-zones has been shown to increase with the degree of cartilage degeneration [31]. Han *et al.* [13] investigated *in situ* superficial zone chondrocytes in order to understand how they can respond to indentation. Chondrocyte deformation under varying strain levels and the effect of anterior cruciate ligament transection (ACLT) on the rabbit patellar AC have been studied since [20, 24, 28]. The biomechanical response of chondrocytes has also been studied (Guilak *et al.*, 1995) in deep, middle and superficial zones, but in this case the samples were full-thickness explants of AC with subchondral bone from the patellofemoral groove [25]. The cell morphology changes at various strain levels were studied more recently (Madden *et al*, 2012) in femoral condyles and patella [20]. Furthermore, accurate determination of the shape, size and orientation of chondrons and chondrocytes in medial condyle tissues has been performed [21].

The motivation to study differences in chondrocyte morphology and mechanical properties among the varying knee joint sites, arises from the fact that differences among sites could help in explaining why some sites of the knee joint may undergo degenerative changes sooner than other sites. For example, it has been observed, that if an experimental osteoarthritis is created by an ACLT procedure, the femoral condyle cartilage of rabbit experiences greatest structural degeneration four weeks after the ACLT [76]. The question this study would answer is that if the differences in cartilage mechanical properties among the sites are related to the chondrocyte behavior under loading.

The aim of this master's thesis is to further investigate the biomechanical response of chondrocytes to deformation across various sites in the rabbit knee joint and link

the mechanical cell responses to tissue scale properties of the AC. The investigation is performed on *in situ* chondrocytes, with the custom built indenter mounted into a stage of a confocal microscope developed by Han *et al.* (2009) [13]. The investigations were performed on six different sites of a rabbit patellofemoral joint, and the changes in chondrocyte morphology were evaluated for each site. The different sites include both femoral condyles, both tibial plateaus, the patellofemoral groove and patella. The specific aims are to investigate if there are site-dependent differences in chondrocyte responses and tissue strains due to tissue loading. Furthermore, it is investigated if there are differences in biomechanical properties of the cartilage among the varying sites, and if the differences could explain observed chondrocyte responses.

Our research hypothesis was that the chondrocytes respond differently to deformation in various tissue sites within the rabbit knee joint and the mechanical responses are related to tissue-level properties of that specific joint tissue site. The remaining chapters of this thesis cover general background, review of relevant literature to this topic, materials and methods, results, discussion and limitations of this study with insight to possible future studies.

Chapter 2

Background

2.1 The articular joint

A joint is a location where bones meet. The type of the joint can be classified by the degree of movement it allows or by the structure of the joint. In this work the knee joint of a rabbit is utilized, which is a synovial joint, also known as a diarthrosis [8].

The joint's main function is to provide a point where movement between the tibia to femur can occur, which is achieved with the help of the patella and fibula. The alignment of bones and the connecting structures are presented in figure 2.1 [9, 10]. Connecting structures consist of ligaments, which are providing stability to the knee by connecting the bones to each other, and tendons which allow the movement of joint by connecting the muscles to the bones [11].

As seen in figure 2.1, the fibula is connected to femur by lateral collateral ligament and the patella is kept in place by quadriceps femoris tendon, which passes over the patella and then continues down to tibia as patellar tendon. The position of patella on the femur is also known as the patellofemoral groove. It is also visible in the figure 2.1 how the femur and tibia are connected by the anterior and posterior cruciate ligaments and by the lateral and medial collateral ligaments. The cruciate ligaments prevent the femur from sliding forwards or backwards on the tibia and the collateral ligaments prevent medial to lateral movement and rotation. [8, 9, 11, 12]

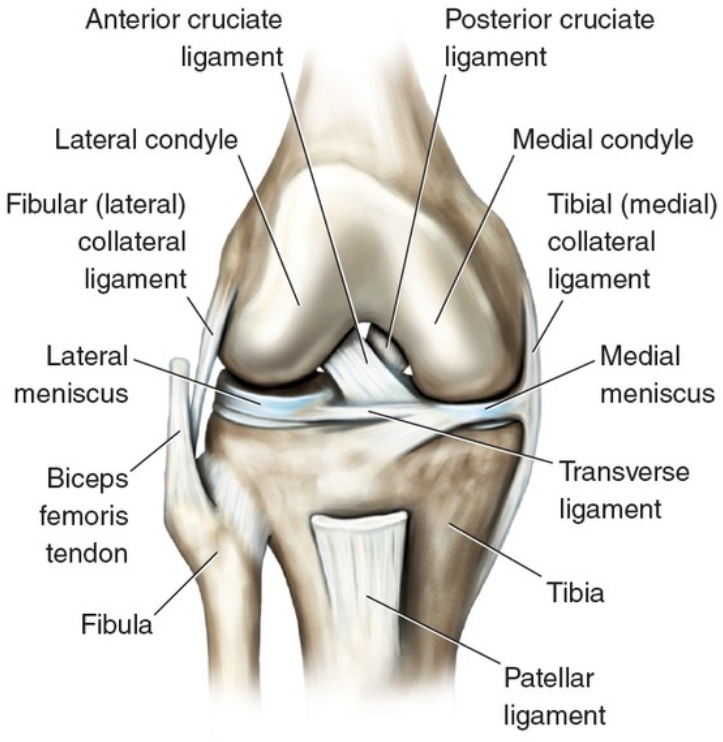

Figure 2.1: Anatomy of the knee. Reproduced with permission from [10].

Femoral condyles and tibial plateaus are not perfectly compatible. For this reason, there are two crescent-shaped pieces of fibrocartilage, called menisci, covering the peripheral regions of the tibial plateaus. Both the lateral and medial meniscus are shown in figure 2.1. In addition to providing stabilization, they also act as a vital shock absorbers and assist in load transmission [12]. In addition to these structures, the knee is surrounded by joint capsule that has synovial membrane. The membrane can secrete synovial fluid, which provides lubrication and nutrition to the joint surfaces [11, 12].

2.2 Articular cartilage

Articular cartilage (AC) is a highly specialized connective tissue found in diarthrodial joints [16]. Its main functions are to provide a smooth gliding surface for connecting bones in the joint, to resists high compressive forces by dissipating the energy associated with the loading and to distribute loads evenly over the whole contacting area [15, 16, 18].

AC has very low frictional coefficient due to synovial fluid and can withstand high shear forces or compressions due to its architecture [16]. The AC's ability to heal is very poor, because it doesn't have blood vessels, lymphatics or nerves and it has low metabolic activity [15, 16]. The avascular status of AC is one of the main reasons why injury healing is quite different in AC compared to some other tissue [18]. The second quite important feature that affects AC modelling is that chondrocytes are trapped in the extracellular matrix (ECM) and are unable to migrate to sites in the tissue which require repairing [18].

2.2.1 Composition

The AC is basically made up of solid and liquid phases. The composition is explained in detail here and values are also presented in table 2.1 [15]. The liquid phase consists of water and dissolved ions. Water is a very important part of the cartilage when it comes to the mechanical behaviour of the tissue. Water takes up 60-80% of the tissue's weight and big portion of the interstitial fluid is free to move under a given load [22]. The flow of water is important because inorganic ions such as potassium, sodium, chloride and calcium are contained in the fluid [16]. In addition to providing nutrition to the chondrocytes through diffusion, the water aids joint lubrication when squeezed out of the AC [16, 18, 22]. The remaining 20-40% of the weight comes from the solid phase. The ingredients of the solid phase are collagen, proteoglycans, glycoproteins and lipids [16, 22]. The collagens make up approximately 65% of the dry weight and proteoglycans make up 25% of the dry weight [22]. The other varying components make up the missing 10% of the dry weight [22]. These percentages vary because they depend on the species studied and also on the location and health of cartilage [37].

Table 2.1: Composition of articular cartilage

Component	Percent of total weight (%)
water	60-80
solid phase	20-40
collagen	15-22
proteoglycans	4-7
glycoproteins and lipids	< 2
Component	Percent of volume (%)
chondrocytes	1-10

Collagens

The term collagen refers to proteins which form a characteristic triple helix of three polypeptide chains. So far 26 genetically different collagens have been described and they vary in size and function [23]. In AC, type II collagen represents 90% to 95% of the collagen in the matrix [16]. Other collagens that are present in the ECM are types I, IV, V, VI, IX, XII and XIV [42]. They mostly provide structural stabilization to the type II collagen network [16], which is responsible for cartilage's strength against shear and tensile forces [15]. Collagen fibrils are cross-linked for further strength, and are linked to proteoglycans via molecular chains: glycoaminoglycans (GAGs) and polysaccharides [70].

Proteoglycan

The proteglycan monomer is made of a protein core (10% of the molecular weight), which has many polysaccharide units called glycoaminoglycans (GAGs) attached to it (90% of the molecular weight). In human cartilage there are two types of GAGs: chondroitin sulfate (CS) and keratin sulfate (KS) [18, 40, 70]. Further, in AC the proteoglycans are mainly of the aggrecan family [41], which can bind with hyaluronic acid (HA) filament forming massive proteoglycan aggregates [40]. The chondrocytes secrete the aggrecan molecules, hyaluronan chain and link proteins, which form connection between these two in the pericellular matrix [43]. The structure of proteoglycan and its metabolic pathway is presented in figure 2.2.

Matrix metalloproteinases (MMPs) cause proteoglycan breakdown and the products are recycled in the endoplasmic reticulum of the chondrocyte [43]. Because proteoglycan aggregates are so large, they are trapped in the collagen interfibrillar space [15]. Furthermore proteoglycans are highly negatively charged, which allows them to retain water effectively. These negative charges of PGs regulate the swelling pressure of the AC to high extent and provide it with the ability to resist compressive loads [16, 26].

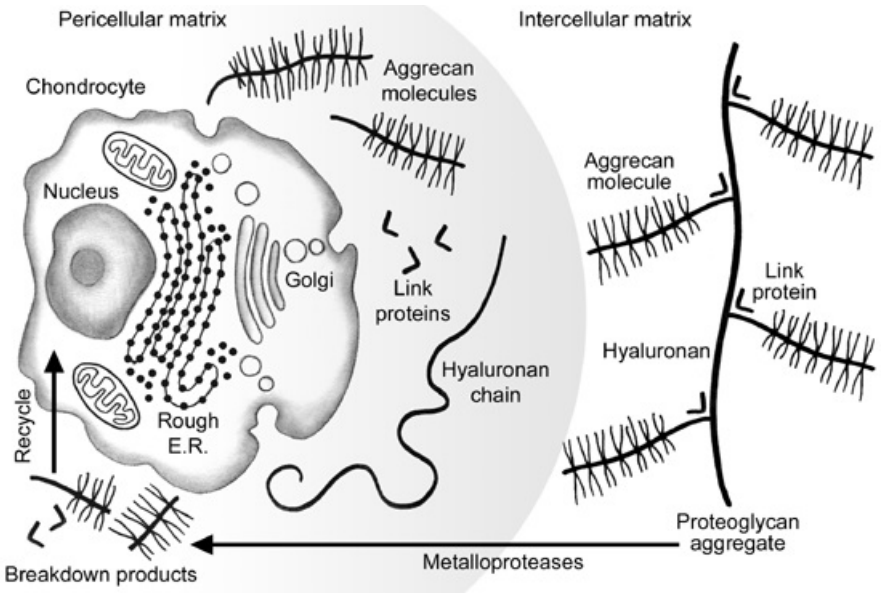

Figure 2.2: Structure of proteoglycan aggregate and metabolism pathway. Reproduced with permission from [43], copyright © Lippincott Williams.

2.2.2 Main structure

AC is composed of chondrocytes, which are embedded within an extracellular matrix (ECM). This matrix is mostly comprised of water, collagen, proteoglycans (PGs) and other noncollagenous proteins [15, 18]. Chondrocytes are the only cells in AC and they are responsible for synthesization of ECM macromolecules (collagen and PGs) and overall maintenance of the matrix [18, 24, 36].

Zones

AC is traditionally divided into four zones based on its composition; the superficial, the middle, the deep and the calcified zone, as shown in figure 2.3 [15, 16, 18]. The relative water concentration in cartilage is highest at the superficial zone, about 80%, and decreases to about 65% towards the deep zone [16]. In cartilage the collagen content is highest at the surface and deep zones, and lower at the middle zone [24]. The proteoglycan content is highest at the deep zone and gradually decreases towards the superficial zone [24].

The superficial zone makes up 10% to 20% of the AC thickness [25]. This zone's main function is to protect the underlying tissue from shear stresses and provide a smooth gliding surface [15, 16]. As seen in figure 2.3 the collagen fibrils in this zone are ordered parallel to the surface and the shape of chondrocytes is very oblate

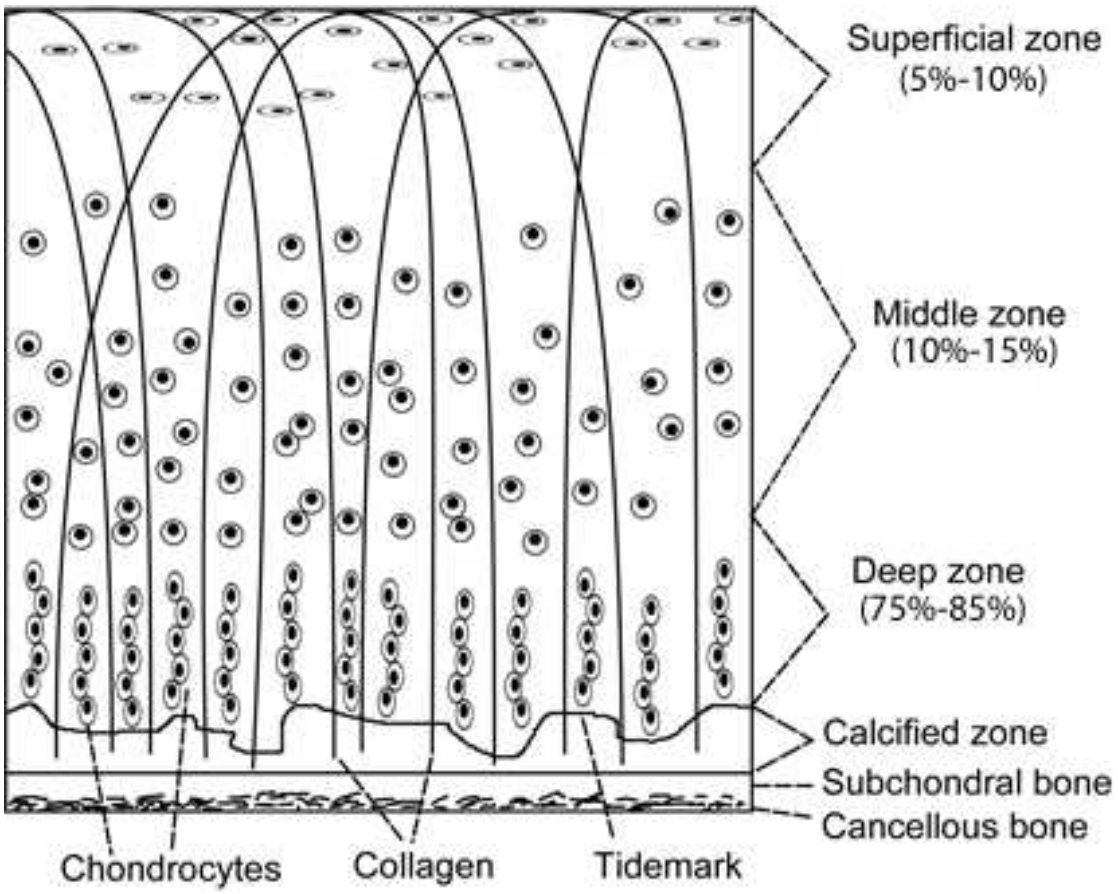

Figure 2.3: Schematic representation of cross-section of articular cartilage showing different zones and zonal arrangement of chondrocytes and collagen. [25]

[16]. The collagen fibrils on the surface follow the so-called "split-line pattern", which follows the direction of joint movement [70]. The split-lines are measured for example by puncturing the cartilage with ink stained needle, which causes the ink to distribute along the preferred collagen fibril directions. Furthermore, in superficial zone the cell density is highest and volume of the chondrocytes lowest [33].

The middle zone makes up 30% to 40% of the whole thickness and functions as a transitional zone between the deep and superficial zones [15, 25]. In addition, the chondrocytes become more spherical and the collagen fibrils are randomly aligned as illustrated in figure 2.3. Also the diameter of collagen fibrils, which ranges in between 30-200 nm [56], is increased compared to the superficial zone [15].

The deep zone makes up rest of the thickness, approximately 40% to 60% [25]. The collagen orientation stays perpendicular to the surface and diameter of the fibrils

becomes larger than elsewhere [17]. The chondrocytes in this zone are arranged parallel to the collagen fibrils in a columnar formation as seen in figure 2.3 [15, 18].

Finally, the calcified zone is separated from the deep zone by a junction of non-calcified and calcified cartilage [57]. This junction is often referred as the tidermark, which represents a calcification or mineralization front. Slow remodelling of the calcified cartilage is reflected as a shift of the tidemark towards the surface of the AC [70]. The collagen fibrils of calcified cartilage provide a fixation between the AC and subchondral bone. The zone also limits diffusion from the bone to the deep zone of cartilage. There are only few chondrocytes in the zone and they are hypertrophic, which means they grow in size and undergo terminal differentiation, which causes also changes in cell synthesis observed for example as type X collagen gene expression [16, 18]. The zone has been considered important for cartilage nutrition and repair because of the close proximity of underlying bone [70].

Regions

In addition to zones, the ECM can be divided into pericellular and extracellular regions [16]. The pericellular matrix (PCM) is a thin region surrounding the chondrocytes. The PCM contains more PGs (e.g. aggrecan, hyaluronan and decorin) than the ECM [16, 18, 58], but the composition is unique because it also contains type VI collagen [21]. The collagen configuration around the cell is presented in figure 2.4. It's thought that during loading the PCM plays a major role in signal transduction and modulates the mechanical forces experienced by chondrocytes [16, 20, 21, 34]. The PCM is also thought to give protection to the cells against mechanical stresses [16, 18]. The PCM and the cells enclosed by it are also called the chondron [21, 58]. An example of single chondron is shown in figure 2.4. The ECM is the largest of the regions and it contains mostly type II collagen and PGs (mostly aggrecan) as explained in previous chapters [21]. The different regions surrounding the chondrocyte can be seen in figure 2.4.

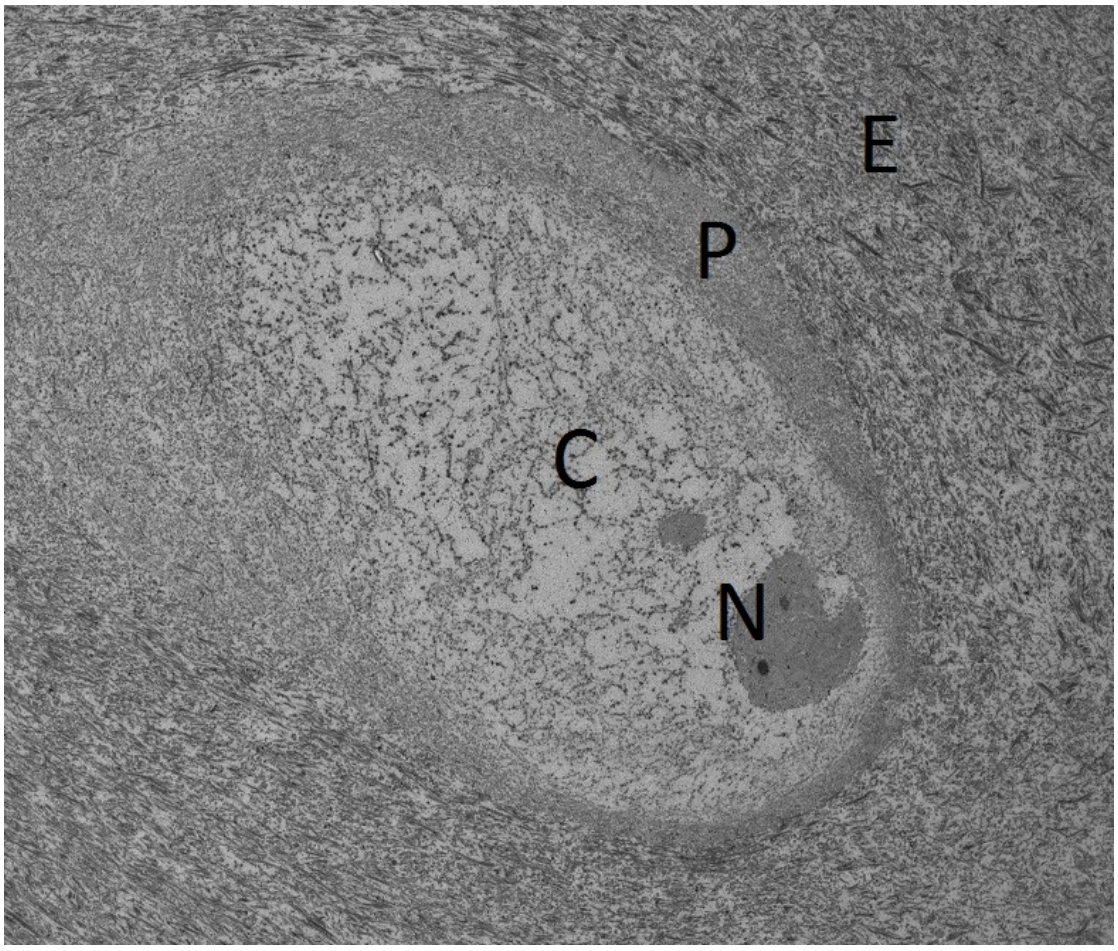

Figure 2.4: A single chondrocyte imaged with transmission electron microscope. C: cell, E: extracellular matrix, N: nucleus and P: pericellular matrix.

2.3 Biomechanics of articular cartilage

The unique mechanical properties of the AC are determined by the collagen-proteoglycan matrix [37] and arise from the fact that this matrix can effectively retain water [16]. The interactions of tissue fluid with the solid matrix give AC its specific mechanical and electro-static properties. Because AC is heterogeneous its functional and material properties also change with the cartilage depth [40, 70].

Collagens have high tensile stiffness, but are thought to have negligible compressive strength. Dynamic compressive forces cause fluid pressurization, which in turn loads the collagen network in tension, and hence leads to the fact that collagen network is providing resistance to dynamic compression [70]. Collagen cross-linking further strengthens the tissue by stiffening the collagen network.

The proteoglycans in the AC have negative electrostatic charge, and hence repel each other. They also cause Donnan swelling pressure. When subjected to compression the repulsive forces between proteoglycans even further increase compared to their pre-tensed state, because the fixed negative charges are forced closer to each other. The electro-static forces between PGs and the Donnan swelling pressure cause the compressive stiffness of cartilage [70].

Fluid in AC is mainly water, but also contains dissolved gas, small proteins and metabolites [70]. Movement of the fluid is hindered by the collagen network and PGs, which make AC to restrain water and act as a porous-permeable material [40]. However, when load is applied to tissue, the fluid will flow with the pressure gradient [70]. Permeability is a measure of the ability of fluid to flow and it is inversely proportional to the frictional drag exerted by the fluid [40]. In cartilage permeability is low ($\sim 10^{-16}\ \frac{\mathrm{m^4 s}}{\mathrm{N}}$) [61], which results in the fact that significant loss of fluid in AC due to compression takes a long time (several minutes) [70]. Because of this, during a loading cycle of e.g. 1 second the fluid flow is negligible. This means that cartilage maintains its stiffness during physiological cyclic loading (e.g. walking) whereas under static loading cartilage becomes softer due to fluid flow [70].

2.3.1 Material properties of articular cartilage

Mechanical properties of AC are different between joints, they change with location within a joint and also vary across the depth of the tissue [61, 70, 71]. Most used methods to evaluate the compressive properties of cartilage include unconfined compression, confined compression and indentation tests [61, 62]. The confined and unconfined tests are carried out on cartilage explants, and indentation tests have been performed on intact cartilage, for example arthroscopically [70]. Schematic illustration of these methods is presented in figure 2.5.

Indentation method gives local response at the specific location of the tissue, whereas confined and unconfined compression give more global response [62]. As seen in figure 2.5, during the confined compression test the sample is in tight impermeable chamber and is loaded with porous indenter, which allows fluid flow out from the sample. In the unconfined geometry the lateral deformation of the sample is allowed, and also the fluid flow is forced into this direction. For confined and unconfined tests, the AC must be stripped off from the underlying bone and

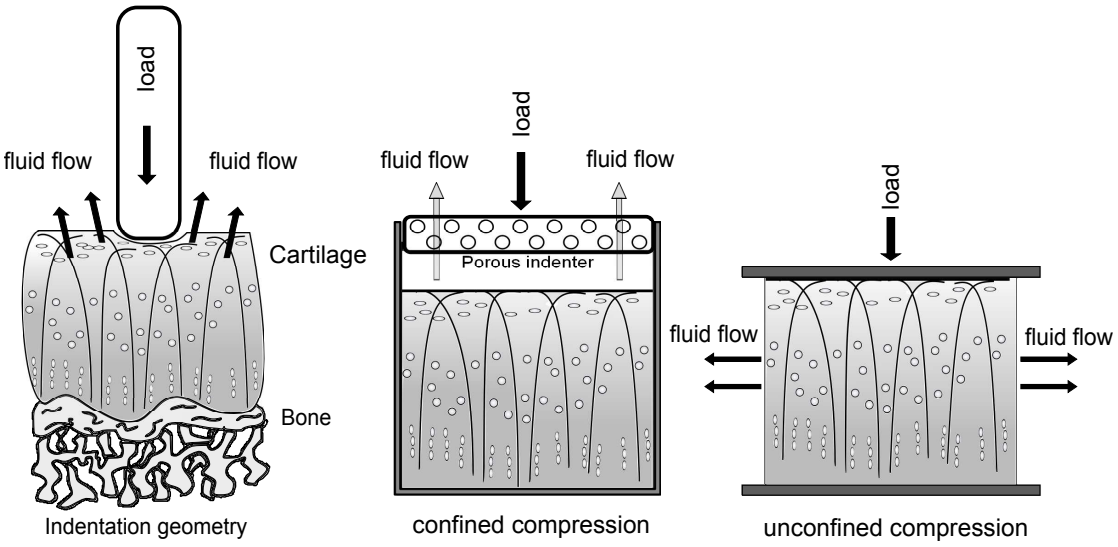

Figure 2.5: Schematic illustration of the three most commonly used techniques for determining articular cartilage mechanical properties in compression.

cut into a perfect cylinder [61]. The major motivation to use indentation over the other two methods is that the measurement can be achieved with minimal disturbance to the samples.

Under compression the AC shows two characteristic responses of viscoelastic materials, creep and stress-relaxation, where material's response to a constant force or deformation varies in time [40]. Hence the two most commonly used compressive tests are creep and stress-relaxation. The viscoelasticity of AC arises from the fluid flow, but it has also been proposed that there are flow-independent components that arises from the matrix properties [70].

In creep testing, a ramp load is applied and deformation response of the tissue is monitored. Creep testing results in a deformation curve presented in figure 2.6. The cartilage responds by initial rapid deformation and continues to deform slowly over time as fluid flows through the porous and permeable matrix until an equilibrium state is reached. In this state the stress developed by the applied load is entirely carried by the solid matrix, when the fluid flow and deformation have ceased [40, 61, 71].

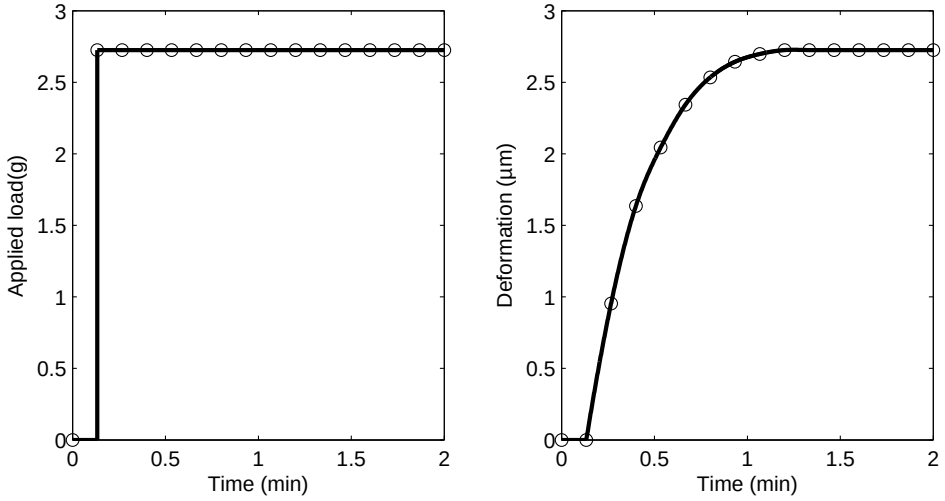

Figure 2.6: Illustration of creep testing of the AC. A ramp load is applied and the subsequential response to deformation is measured.

In stress-relaxation testing, the applied deformation is constant and the stress changes are monitored. An illustration of both deformation and stress curves of cartilage during stress-relaxation testing is presented in figure 2.7. During the initial compression phase, the stress rises until the deformation is at its peak. After that, the stress decays until an equilibrium stress is reached [40, 61]. The sharp rise is associated with fluid exudation, while the stress-relaxation behavior happens because fluid redistribution within the matrix and out of the tissue [71].

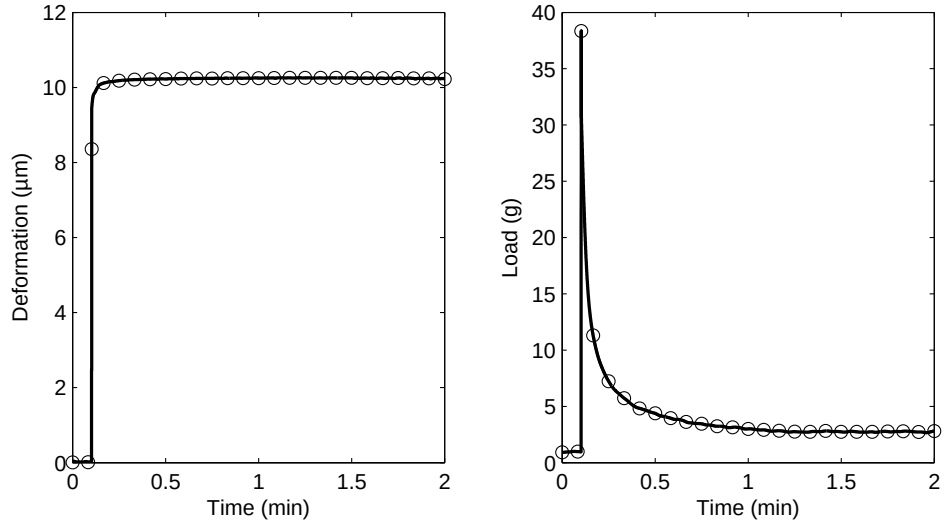

Figure 2.7: Illustration of stress-relaxation testing of the AC. A ramp deformation is applied and the subsequential load is measured with the indenter.

The compressive equilibrium properties of AC are tightly linked to PG content, whereas the dynamic properties are affected by the fluid and collagen network. The superficial zone has the lowest PG content, highest permeability and hence deforms most during equilibrium compression [15]. Orientation of the collagen fibrillar network may also affect the stiffness, because changes in stiffness observed experimentally cannot be explained by the rise in PG content alone [70]. The superficial zone integrity is essential in the protection and maintenance of deeper layers. This zone also is responsible for most tensile properties of the cartilage, which are contributing to the resistance of shear, tensile and compressive forces imposed by articulation [16]. Experiments show that middle zone functionally resists compressive forces [16], but the deep zone is responsible for providing the greatest amount of resistance to the compressive forces [16].

The tensile properties of cartilage are also important, because dynamic compression of cartilage generates significant tensile stresses [40]. The network of collagen is primarly responsible for the tensile properties of the cartilage [40, 70, 71]. The tensile strength of the AC is highest at the superficial zone and decreases with increasing depth in the tissue [70]. Tensile strength is also direction-dependent, being higher along the split line, i.e. the collagen long axis direction, than perpendicular to it [70].

In tension, the deformation response of the AC is nonlinear and highly anisotropic [71]. This is caused by the fact that collagen tends to 'stiffen' with increased tensile stress [71]. The tensile stresses caused by deformation are illustrated in figure 2.8. At first, in the toe region, small loads cause large deformations, which can be explained by uncrimping of the collagen fibers. The stress comes from the force required to slide the collagen meshwork through the PGs [40]. After the collagens become taut, the AC becomes linearly elastic, and the load is carried primarily by the collagen fibers, until failure occurs [71].

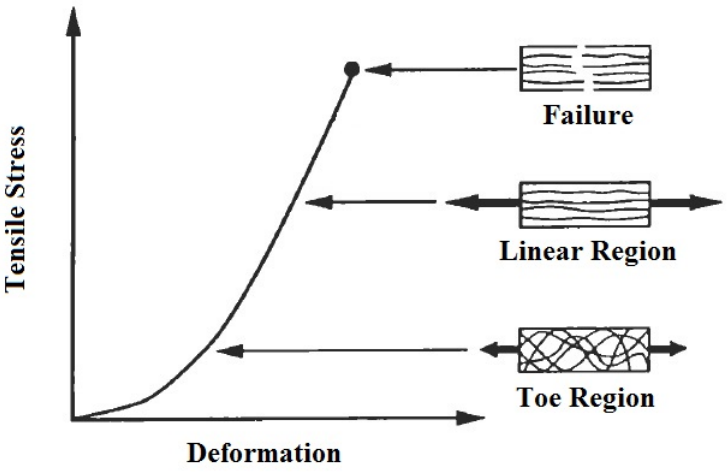

Figure 2.8: Schematic representation of tensile stress development under deformation. The configuration of collagen fibers in each strain region is also shown. Reproduced with permission from [40], copyright © Journal of Orthopaedic & Sports Physical Therapy®.

2.3.2 Mechanical parameters

Strain is a measure of relative change in length, for cartilage the global strain ϵ is calculated as the change in thickness due to tissue compression (ΔH) divided by the original tissue thickness (H). Similarly, nominal stress (σ) is calculated as force (F) divided by the cross-sectional area (A), which the force is applied over. The elastic modulus E, also known as Young's modulus, of the cartilage sample is defined as:

$$E_{measured} = \frac{\sigma}{\epsilon} = \frac{F/A}{\Delta H/H} = \frac{FH}{A\Delta H}. \tag{2.1}$$

The use of an elastic model may be used for the study of instantaneous or equilibrium response, when fluid flow is small or absent [70]. In case of indentation measurements, the following formula [52] for an isotropic elastic material with the assumption of a frictionless indenter has been derived for AC:

$$E = E_{measured}\left(\frac{\pi r}{2H\kappa}(1-\nu^2)\right). \tag{2.2}$$

Here r is the indenter radius, H is the cartilage thickness, κ is the novel scaling factor (function of aspect ratio r/H) and ν is the Poisson's ratio. The value of scaling factor κ as a function of aspect ratio is shown for two values of κ in table 2.2 provided by Zhang *et al.* (1997) [63]. The two values of Poisson's ratio ($\kappa = 0.2$ and $\kappa = 0.5$) were used in this study to investigate the equilibrium and

dynamic response, respectively. Furthermore, the values presented in table 2.2 assume isotropic elastic material, but also consider friction between the indenter and sample.

Table 2.2: Values of κ for a flat-ended cylindrical indenter with a diameter of 1 mm.

Aspect ratio (r/H)	$\nu = 0.2$	$\nu = 0.5$
0.2	1.212	1.244
0.4	1.479	1.698
0.6	1.755	2.183
0.8	2.055	2.800
1.0	2.371	3.590
1.5	3.222	6.078
2.0	4.058	9.110

From stress-relaxation measurements of few cycles (e.g. 3 steps at 5% strain) the Young's modulus is calculated at the equilibrium as following: a line is fitted with linear least squares to points (ϵ, σ_∞), where σ_∞ is the stress value at equilibrium (see figure 2.7). Now the slope of the fit equals Young's modulus according to equation (2.1). Then the values are corrected according to equation (2.2), which gives the equilibrium modulus (E_{eq}).

The dynamic modulus of cartilage is similar to elastic modulus, but the difference is that in a viscoelastic material, like cartilage, there is storage and loss of energy that is considered. The stored energy is caused by the material's elasticity, and the loss of energy by viscosity, where energy is dissipated to surroundings as heat. This causes phase lag φ between the strain and stress. With this in mind the equations for strain and stress can be written as

$$\epsilon = \epsilon_0 \sin(t\omega) \tag{2.3}$$

$$\sigma = \sigma_0 \sin(t\omega + \varphi). \tag{2.4}$$

Here ω is the frequency of oscillation and t is time. Now the storage and loss of elastic moduli can be calculated as

$$E' = \frac{\sigma_0}{\epsilon_0} \cos\varphi \tag{2.5}$$

$$E'' = \frac{\sigma_0}{\epsilon_0} \sin\varphi. \tag{2.6}$$

The dynamic modulus is now defined as a modulus of a complex number:

$$E_{dyn} = |E^*| = |E' + iE''| = \sqrt{E'^2 + E''^2} = \frac{\sigma_0}{\epsilon_0}\sqrt{\cos^2\varphi + \sin^2\varphi} = \frac{\sigma_0}{\epsilon_0}. \quad (2.7)$$

The dynamic modulus is usually calculated as an average of, for example, four cycles of indentation. In case of the indentation geometry the dynamic moduli are first calculated according to equation (2.1) and then fixed with (2.2) using $\nu = 0.5$ (for an incompressible material) [76].

2.4 Osteoarthritis

Osteoarthritis (OA) is the most common joint disease, and the early phase of the disease is associated with degeneration of the cartilage surface, osteophyte formation, changes in the subchondral bone and swelling and pain in the joint [28, 35]. The disease usually progresses slowly, but in the late stages total erosion of cartilage occurs, which may lead to total joint immobilization due to pain. Furthermore, there are no pharmacological treatments available that could halt or slow down the progression of OA [30]. Instead, the drugs are used to reduce pain or inflammation of the joint [51].

The first signs of OA include surface fibrillation, development of lesions across the joint surface and clefts that propagate from the surface of the AC into the tissue depth [37]. Compared to the collagen content, which stays mainly the same, the PG content seems to decrease during early OA [24]. The collagen network fibrillation causes swelling, because of the decreased resistance to prevent the swelling pressure caused by the PGs. As a response to these changes, the synthetic activity of chondrocytes is increased, which causes accelerated breakdown of the ECM and macromolecules [50]. However, after a while the reparative response of chondrocytes weaken, leading to a decrease in collagen and PG content and the development of full-thickness clefts [50].

Moreover, it is known that in OA there is an imbalance between catabolic and anabolic activities within chondrocytes [30]. In healthy cartilage the catabolic activity takes care of damaged tissue removal and anabolic activity replaces the damaged tissue [38]. Breakdown of the ECM is at least partly mediated by up-regulated expression of proteolytic enzymes [30]. These enzymes include MMP-3,

8 and 13 (matrix metalloproteinases), which can cleave type II collagen, and proteoglycan aggrecanases, particularly ADAMTS-1, 4 and 5 (A Disintegrin And Metalloproteinase with Thrombospondin Motifs) [30, 50].

The levels of active ADAMTS and MMPs are suppressed partly by TIMPs (tissue inhibitors of metalloproteinases) in normal tissue turnover, but in OA the increased activity of proteolytic enzymes takes over resulting in the breakdown of AC [30]. The MMPs are proteinases, which are enzymes capable of breaking down peptide bonds, that link amino acids together and ADAMTS are aggrecanases, which can break down cartilage aggrecans [50]. TIMPS are proteins capable of inhibiting the activities of all known MMPs and because of this, have a key role in maintaining the metabolic balance of the ECM [59].

Even today, physical activity remains the most widely used non-pharmacological method in the management of OA, but the detailed mechanisms that cause the benefits of physical therapy are poorly known [30]. Other non-pharmacological methods include a variety of physical rehabilitation methods (e.g. thermal therapies or electrical stimulations), behavioral intervention and alternative treatments, such as homeopathy, herbs and acupuncture [51]. All these treatments can help to reduce the general patient suffering, but the benefits are not guaranteed or supported by scientific data. Surgical intervention is usually only considered in cases in which the other treatment methods have failed. There are different surgical treatments available with replacement of the whole joint with an endoprosthesis being the last option [51].

2.5 Animal models used in cartilage research

The changes that happen in AC during the OA are known, but the initiation and progression of AC degeneration aren't. Human tissue is very rarely available for the study of early OA progression. This arises from the fact that treatments of early OA cause minimal invasion to the joint and rarely include removal of the AC, and also patients do not seek treatment to OA until the progression of the disease causes joint pain and dysfunction [31]. Because of the low availability of human tissue, animal models are widely used in studies of AC and OA.

Surgery is the most widely used method to induce OA in animal models, because it causes changes in the mechanical loading patterns of the joint. This causes

advantages like progressive and predictable disease onset, molecular pathology of the OA and the surgical procedure can mimic corresponding human injury [46]. Partial and total menisectomy and anterior cruciate ligament transection (ACLT) are the most widely used methods to surgically induce OA in animal models [45, 47]. These procedures have been successfully carried out on dogs, rabbits, sheep, cows, cats, and smaller animals like guinea pigs, rats and mice [45]. Other methods to cause OA in animal models include immobilization, intraarticular injections and spontaneous development of OA [46].

Injections to induce OA can be enzymes (collagenase, hyaluronidase), cytokines (IL-1) or transforming growth factors (e.g. TGF-β). The collagenases break the collagen peptide bonds, the hyaluronidase degenerates hyaluronic acid and hence also the PGs, the cytokines are mediators of inflammation and the TGF-β is a protein that controls for example cell growth and cellular differentiation [50]. The downside with injections is that they usually cause local inflammation and selective degradation of the ECM components, which poorly replicates the OA disease process [46]. Immobilization produced changes can mimic OA pathology, but some differences are observed in chondrocyte morphology, such as excess necrosis and lack of cell cloning. Furthermore the immobilization causes nutritional deprivation due to the absence of loading and fluid movement [46]. Spontaneous OA occurs within a reasonable time frame in genetically modified mice, macaques and guinea pigs. The advantage with these models is naturally occurring disease, but the time frame of disease progression is varying and the underlying mechanism causing the disease might not be the same as in human OA [46].

2.5.1 Interspecies and regional differences in the knee joint

Anatomical differences are obviously present between different species, for example between human and rabbit. Still it has been shown, for example for the femoral condyle and femoral groove, that no differences in the tissue equilibrium modulus among different species including bovine, human, dog, monkey or rabbit exist. This does not include the femoral groove of rabbit, which undergoes higher loads due to a normal knee flexion of 135°. Furthermore, no correlation has been found between equilibrium modulus and tissue thickness of the test sites. [69]

The low-weight-bearing areas of AC have lower PG content and higher collagen content, when compared to regions undergoing higher loads [69]. The higher PG

content causes the sites that experience higher loads to have greater compressive moduli in equilibrium. The collagen content and orientation controls the dynamic compressive modulus. All species mentioned before, except humans, exhibit the highest equilibrium modulus in AC from a region of the medial condyle, however for humans the highest modulus of AC in the knee joint is from the lateral condyle [69].

2.6 Chondrocytes

As mentioned before, chondrocytes are the only cell type found in the AC. Their function is to maintain the matrix health by producing the macromolecules, collagen and PGs, and they also are responsible for the extracellular matrix integrity [18, 24, 29]. Chondrocytes are softer than the ECM by a factor of about 1000 [70]. Therefore, they should deform much more during loading than the ECM, but this does not neseccarily happen, because the chondrocytes are protected by the PCM and pericellular capsule [70].

It is established that chondrocyte volume and morphology changes under mechanical stress and also during progression of osteoarthritis (OA) [24, 25, 35]. In OA, the osmolarity of the ECM becomes hypotonic, which leads to increased chondrocyte volume [35]. Furthermore these changes are inhomogeneous through the depth of the tissue [25, 34]. In addition to properties of the ECM, the collagen fibrils of the ECM have an influence on local strains and volume changes of the chondrocytes during loading [34].

2.6.1 Structure

Chondrocytes are surrounded by a hydrophobic plasma membrane (lipid bilayer) that separates the extra- and intracellular environments [26]. Only small lipid-soluble molecules such as oxygen, water and carbon dioxide are able to penetrate this lipid bilayer, which is a thin membrane made of two layers of lipid molecules. Other molecules can be taken into or pumped out of the cell by transmembrane protein channels and transporters [26, 27]. The transporters can move substances passively or actively. Active transport happens against the electrochemical gradient and requires energy, which is primarly derived from hydrolysis of adenosine

triphosphate (ATP) [26, 27]. The last way molecules can enter the cell is through endocytosis, where the plasma membrane traps the molecule and deforms inwards until it is within the cytoplasm and then the deformation 'snaps' creating a vesicle containing the molecules. This can occur also to other direction and in that case the phenomenon is called exocytosis [27].

The cytoskeleton of chondrocytes, which is composed of actin, microtubules and intermediate filaments (IFs), contributes to the cell's shape, movement and structural integrity [36]. Microtubules are composed of protein called tubulin, and are largest of these three, having a diameter around 25 nm. Actin filaments are made of protein called actin and have a diameter of only 6 nm. The intermediate filaments are constructed from different subunit proteins and are medium sized, having diameter of about 10 nm [60].

Actin filaments are involved in cell movement and cytokinesis. The IFs are strong and ropelike, and their functions are primarily mechanic, but they are not as dynamic as actin filaments [60]. Actin and IFs may play an important role in mechanical properties of the chondrocyte. For example, it has been shown that chemical disturbance of these filaments leads to a decrease in mechanical stiffness of human chondrocytes [36].

2.6.2 Mechanotransduction

Chondrocyte activity is thought to be connected to factors like composition of the ECM, environmental and genetic effects and mechanical stimuli [28]. The manner in which the loading of the AC is converted to chemical signals within the chondrocytes and how these signals cause alterations in macromolecule turnover is called mechanotransduction [26]. This mechanotransduction is initiated at the interface between the ECM and the cell membrane [30]. It is known that the composition (PG, water and collagen content) of the pericellular matrix (PCM) can alter the deformation behaviour of chondrocytes [16, 18, 22, 29, 34].

Cell mechanoreceptors such as mechanosensitive ion channels and integrins are recognizing physiochemical changes [38]. Mechanical stimuli leads to the activation of both stretch-activated and voltage-dependent ion channels, which cause activation of signalling pathways in chondrocytes by allowing influx of ions such as calcium. The integrins are transmembrane glycoprotein receptors, which are

attached to actin cytoskeleton and the ECM. In cartilage, the $\alpha5\beta1$ integrin is the most important of these molecules [38]. In addition, mechanical stimuli causes the chondrocytes to release soluble mediators that activate cell surface receptors [38].

Dynamic loading of the AC tissue causes increase in hydrostatic pressure, fluid flow and matrix deformation. These changes have been linked to cause aggrecan and protein synthesis by the chondrocytes [26]. In case of static loading, osmolarity and ion concentration of the ECM are increased and pH of the tissue is decreased. Chondrocytes tend to decrease their metabolic activity due to these changes in the ECM [26, 29, 38]. Furthermore, static loading and mechanical loading with injurious pressures causes production of various matrix metalloproteinases, aggrecanase-1 and matrix protease regulator cyclooxygenase-2 (COX-2) [38]. Static loading also decreases collagen II and aggrecan gene expression, which is caused most likely by stimulation of interleukin-1 (IL-1) receptors [38].

The type of loading does not solely define the cell response, but also the amplitude, frequency and duration of the load must be taken into account [26, 36]. For example, under impact loading of bovine cartilage surface, there appears to be a critical threshold of 15-20 MPa, which leads to cell death and collagen damage when applied on cartilage explants [39]. Furthermore, in other study pressures between 7-12 MPa caused collagen degradation and peak stresses as low as 4.5 MPa caused chondrocyte apoptosis [39]. Also, even without compression the biosynthetic activity of chondrocytes differs between zones, being higher at the deep and middle zones compared to the surface [33]. Furthermore, it is good to note that in healthy AC the chondrocytes replace ECM material quite slowly. It has been approximated that collagen half-life would be over 100 years, and respectively it has been estimated that half-life of the aggrecan GAG chains is in the range of 3-24 years [5].

One of the mechanotransduction pathways in chondrocytes consists of Ca^{2+} signaling. Although the mechanisms are not completely understood, it is known that physical stimuli, fluid flow, hydrostatic pressure and osmotic stress all influence this Ca^{2+} signaling [44]. Anyhow, calcium signalling is important, because it regulates cell metabolism, proliferation, gene transcription and contraction [44]. The mechanotransduction pathway of Ca^{2+} is illustrated in figure 2.9. The mechanical forces cause influx of Ca^{2+} by activation of stretch activated ion channels (SAC), and the $\alpha5\beta1$ integrin, which is associated with a CD47 protein, which is further involved in elevation of aggrecan gene expression [38]. The mechanical stimuli also

causes release of soluble neuropeptide substance P from the cell, which is known to act through the neurokinin 1 (NK1) receptor to induce interleukin-4 (IL-4) release [38]. The IL-4 receptor causes intracellular signalling cascades with Ca^{2+}, that lead to activation of calcium-activated potassium channels (SK channel) and regulation of gene expression, which finally leads into production of matrix proteins or proteases [38].

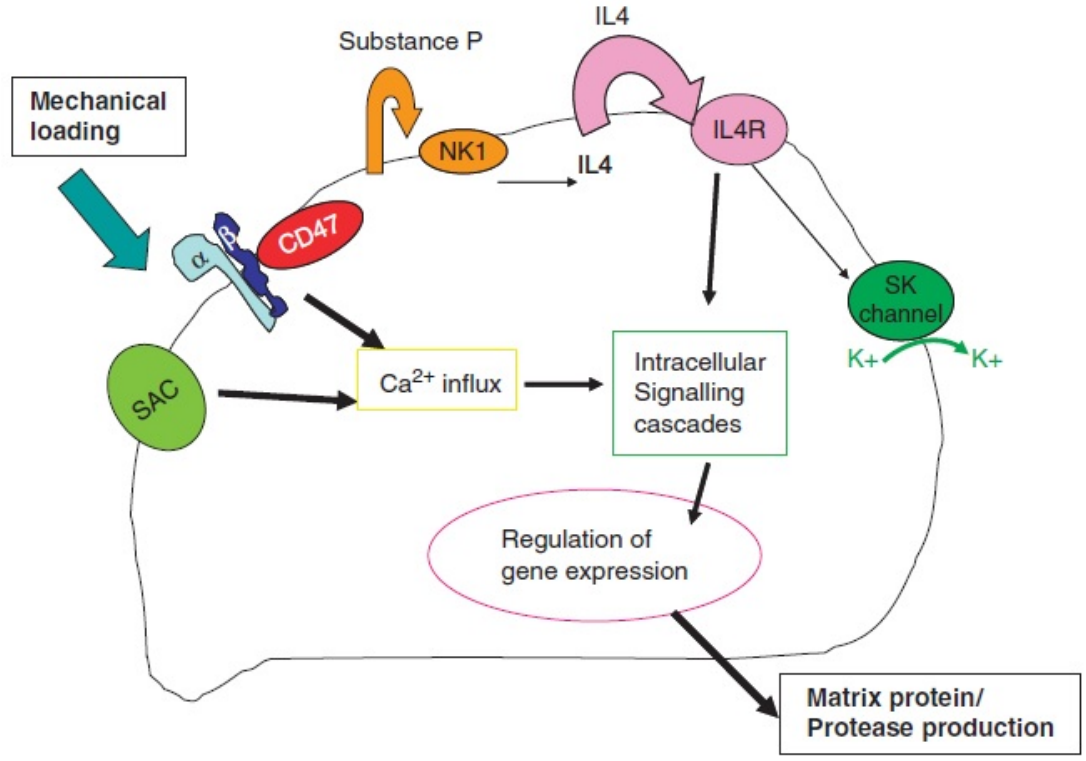

Figure 2.9: Illustration of mechanotransduction pathway by Ca^{2+} signaling. Reproduced with permission from [38], copyright © John Wiley & Sons A/S.

2.7 Confocal laser scanning microscopy

The principle of confocal imaging is that the confocal microscope uses point illumination, which is achieved with a pinhole in front of the light source and the detector to eliminate out-of-focus signal [75]. In this study we used fluorescence imaging, and the samples were stained with a fluorescent dye. The fluorescent stains can be molecules that bind for example covalently to the molecule of interest. Common factor with all the dyes is that they undergo fluorescence when illuminated.

Fluorescence is emission of light from the sample, which is caused by absorbtion of electromagnetic radiation (photons). The absorbed photon raises an electron of the dye to an excited state, which dissipates a little of its energy by molecular collisions and then returns to the ground state and emits a photon with less energy than the absorbed photon [73]. The emitted photons from sample are collected with a detector and image is formed.

The working principle of confocal microscope is shown in figure 2.10. The fact that in fluorescence imaging the illuminated light usually has smaller wavelength than observed light, makes it possible to use dichromatic mirror, which transmits one wavelength and reflects the other. In ideal case this means that all the illumination light reaches the sample and no fluorescence light is lost on the way back to detector [73]. The unwanted wavelengths can be further suppressed by adding barrier filters that only let specific wavelengths through. The importance of pinholes to suppress unwanted out-of-focus light can also be seen from the figure 2.10.

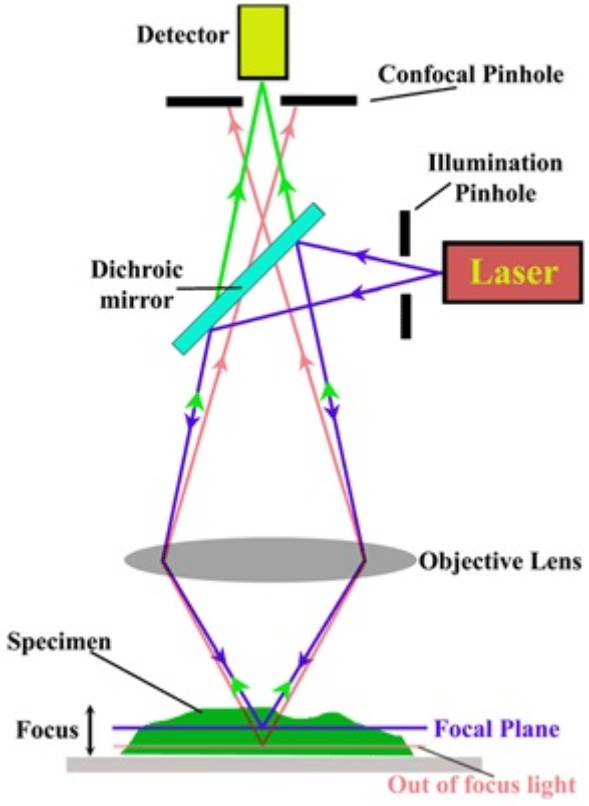

Figure 2.10: Working principle of confocal microscope. Reproduced with permission from [72], copyright © John Innes Centre.

In traditional wide-field fluorescence microscopy the entire specimen is illuminated evenly and all parts of the specimen are excited at the same time and the resulting

fluorescence is detected. The confocal microscopy uses point illumination and the light produced by fluorescence is only detected from the chosen focal plane. This leads to much higher optical resolution when compared to wide-field microscopy. Furthermore, confocal microscopy provides the ability to image also in the depth direction, which is flooded with light in normal wide-field fluorescence microscopy. [75]

The drawback is that only small focus can be imaged at once, which means that scanning is required to form 2D or even 3D images of the sample [75]. The scanning is usually performed with oscillating mirrors, and is done point-by-point and line-by-line basis at certain tissue depth [66]. Another drawback is that the signal intensity is decreased due to the two pinholes, which leads to longer exposure times and photobleaching. However, the fact that the sample preparation is simply staining the sample with fluorescent dye and the samples can be imaged *in situ* without any fixation or disturbtion, makes the method very common when imaging for example living cells [66]. Also the benefit of being able to go into the depth direction of samples makes this imaging method suitable for example in imaging the chondrocytes of the superficial zone articular cartilage [25].

However, confocal laser scanning microscopy (CLSM) causes photobleaching artifacts that lead to a decrease in fluorescence intensity and reduce the image contrast [66]. The photobleaching is caused by the fact that the fluorescent agents are excited along the light path, even though the light illuminated by them is not shown because it is eliminated by the confocal pinhole [66]. For this study, the important thing is that the photobleaching causes errors in chondrocyte volume determination, which are of the magnitude of $< 5\%$ [66]. This scale of error is negligible to this study and might be even less because the scans were not performed many times and the photobleaching was not intentionally caused like in the study of imaging errors by Moo *et al.*, 2013 [66].

Chapter 3

Relevant literature and significance

The deformation of chondrocytes under load has been extensively studied before, including isolated chondrocytes [64], chondrocytes in agarose gel constructs [65] and chondrocytes in tissue explants [21, 25, 31]. The behavior of chondrocytes under deformation in their physiological environment, surrounded by intact PCM and ECM, is poorly known in different sites of the knee joint. Furthermore, it is known that the chondrocytes are greatly influenced by the solid matrix, and specifically if it is intact or has been compromised, like in cartilage explants [20].

The evaluation of isolated chondrocytes and chondrons has shown that chondrons are generally stiffer and show less viscoelastic behavior than chondrocytes, which implicates that the PCM significantly influences the mechanical behavior of the cells [64]. In cartilage explants, the morphology of chondron varies within AC depth, reflecting the local collagen architecture [21]. In the gel constructs static and dynamic loading has been compared and found that cell deformations were reduced over 20 minute period of cyclic compression, while they stayed constant during a static compression, suggesting that cyclic loading alters cell response [65].

In cartilage explants it has been shown that chondrocytes deform during compression within the surface, the middle and the deep zone, but the change in volume of cells is the largest within the surface zone [25]. Furthermore the lateral expansion of chondrocytes is anisotropic and cells deform more perpendicular to the

local split line pattern [25]. Also the cell swelling within the superficial and mid-zones has been noticed to increase with cartilage degeneration, implicating that cell volume increases may indicate early OA-like changes occurring in AC [31].

A custom built indenter mounted into a stage of a confocal microscope developed by Han *et al.* (2009) [13] has been previously used to study chondrocytes under extreme strains [20] and chondrocyte behavior after an ACLT [24, 28]. Deformation-induced chondrocyte volume changes were positive (increasing cell volume) in both studies [24, 28] after an ACLT procedure (4 and 9 weeks), while in control group the deformation of cartilage caused chondrocyte volume decreases. This indicates that progression of OA is altering the biomechanical response of chondrocytes to compression. In the study by Turunen *et al.* (2013) [24] it was noted that collagen content between ACLT and contralateral cartilage was similar, but the PG content of the ACLT cartilage was reduced and the collagen orientation angle of the ACLT cartilage was increased when compared to contralateral cartilage in the superficial layer. Furthermore, the expansion of chondrocytes in the ACLT cartilage could be explained by altered PCM and ECM surroundings, which would allow larger cell expansion and the increase in cell volume due to compression [24]. This would indicate that the local structure is driving the cell mechanobiological response of the chondrocytes. This hypothesis is further backed up by the observation that cells deform anisotropically in the superficial layer preferring the direction perpendicular to the local split-line pattern as observed by *Guilak et al.* (1995) [25].

Tanska *et al.* (2013) used a multiscale fibril-reinforced poroelastic swelling model to study if the experimentally observed volume increases due to an ACLT can be explained by changes in the ECM and PCM properties [68]. It was observed that the increased cell volume after loading could be explained by the reduction of PCM fixed charge density (PG content), while the reduced collagen stiffness would only be a secondary contributor to the increased volume [68].

In study by Madden *et al.* (2013) the deformation of chondrocytes under various strains were investigated on the femoral condyles and patella taken from the rabbit knee joint [20]. It was observed that at low levels of applied ECM strains, these were higher than tissue strains, but at extreme levels of ECM strains these were smaller than the tissue strains. Additionally cell compressive strains were always lower than applied tissue strain. Significantly smaller strains were also observed in the tissues than previously found strain levels in hemi-cylindrical explants,

which implies that studying chondrocyte deformation responses in the native tissue environment is crucial for linking cell based deformational changes to tissue-level deformation. This arises from the fact that in explant tissues both the architecture and the integrity of the ECM is altered and hence the function of the matrix is compromised, which leads to an overestimation of cell level deformation. Also it was seen, that the local ECM and pericullar matrix (PCM) structure are protecting or shielding the cells at high tissue loads.

Recently Mäkelä *et al.* (2014) investigated biomechanical properties, composition and structure of rabbit knee joint tissues. These were examined in a site-specific manner, covering tibial plateaus, femoral condyles and femoral groove tissues [76]. The samples were harvested from rabbits that underwent an ACLT procedure (post 4 weeks), from the contralateral knees of these rabbits and from healthy control rabbit knees. The study was focused on determining the differences between ACLT and the control tissues and it was seen that the femoral condyle cartilage underwent most dramatic changes due to the ACLT procedure. For the interest of this study, there were also differences in the equilibrium and dynamic moduli among the sites in the control samples [76]. However, the chondrocytes were not investigated in this study.

Overall, the studies that have been performed have usually investigated cell-level or tissue-level parameters from a single location or from a few locations within the knee joint. Our study tries to fill this gap of information by measuring the mechanical response of chondrocytes to deformation and also by measuring tissue-level parameters, strains and determining mechanical tissue properties across various sites within a rabbit knee joint.

The hypothesis of this study is that superficial zone chondrocytes from the different sites in the rabbit knee joint respond differently to deformation. This, in turn would also drive differences in biomechanical responses of the joint tissues. Furthermore, it is thought that tissue structural variations and different functional requirements of the joint tissues may drive cell biosynthesis and alter the ECM and PCM properties between different tissue sites.

The significance of this study is that we link the tissue-level strains and mechanical moduli to the cell-level morphological changes and do this in site-specific manner over the whole rabbit knee joint. The measured values will also act as a solid reference for future studies about deformation-induced cell morphology changes within

the rabbit knee joint. Such studies could be for example how altered mechanical loading patterns (e.g. ACLT or menisectomy or even a partial menisectomy) of the knee joint may cause differences in mechanical responses of chondrocytes between different tissue sites.

Chapter 4

Materials and methods

4.1 Confocal laser scanning microscopy experiments

A custom-made indentation system developed by Han *et al.* (2009) built into a confocal laser scanning microscope (CLSM) was used to extract 2D image stacks of the articular cartilage [13]. The picture of the used CLSM system and an example of imaged 2D image stack can be seen in figure 4.1.

The flat-ended indenter was made of glass to enable transmission of light and it was mounted along the optical axis of the CLSM (LSM 510, Zeiss Inc.). The indenter was in enclosure fixed on custom motorized x-y stage. Mechanical loading was achieved by pushing the sample against the fixed indenter to avoid any movement of the x40-magnification objective (40 x 0.8 NA water-immersion objective, Zeiss Inc.).

The indentation system is presented in figure 4.2. The system was build under the sample holder and it consists of piezo actuator (FPA-2000, DSM, TN, USA), load cell (ELW-D1, Entran, VA, USA) and linear displacement gauge (HMG-DVRT-1.5, MicroStrain, VT, USA). The actuator controls the movement of the sample holder, the load cell measures the contact force on the sample surface and the DVRT (Differential Variable Reluctance Transducer) measures the displacement of the sample relative to the indenter.

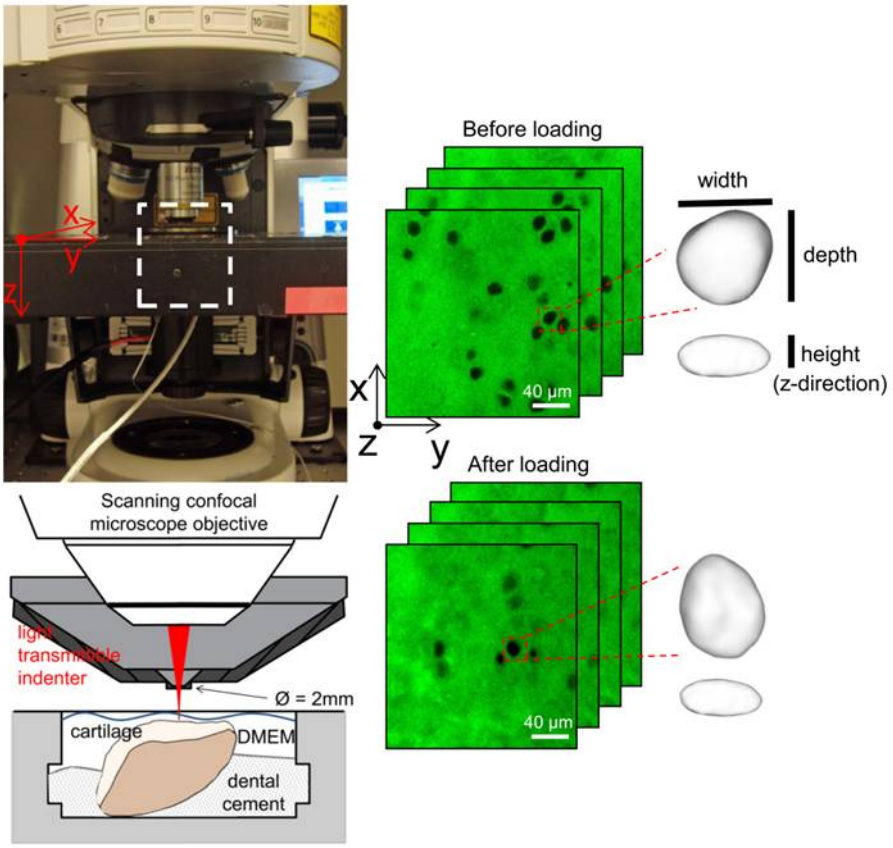

Figure 4.1: CLSM system components and a 2D image stack. Both the indenter and the indentation system are in an enclosure. The sample was bathed in Dulbecco's Modified Eagle's Medium (DMEM) and fixed using dental cement. Same chondrocytes were cropped from before and after loading images for dimensional analyses.

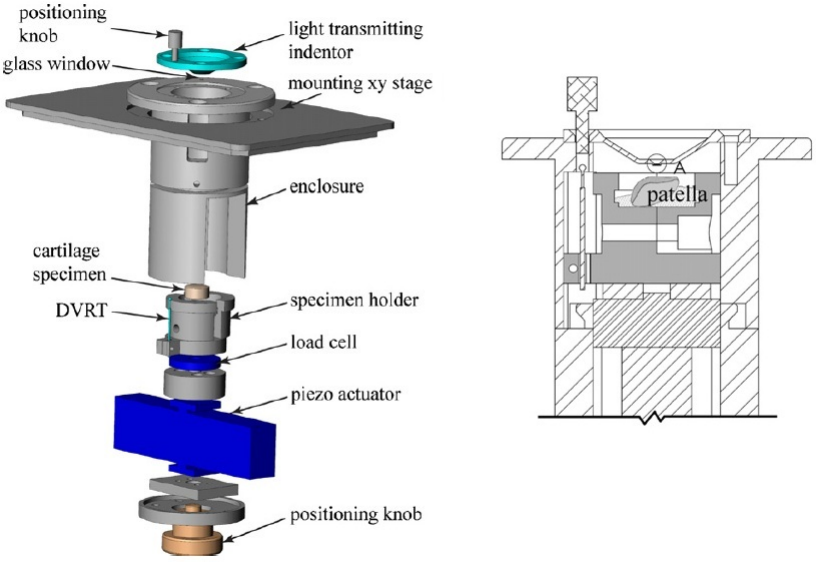

Figure 4.2: Indentation system of the CLSM. Reproduced with permission from [13].

4.2 Samples and measurements

Five skeletally mature (13 ± 1 month) female New Zealand white rabbits were sacrificed for the study and their knee joint tissues were harvested. The procedure was performed according to the guidelines of the Canadian Council on Animal Care and was approved by the committee on Animal Ethics at the University of Calgary. Excess tissue was removed while keeping joint surfaces and underlying bone intact. Joint tissues were stained with conjugated fluorescent Dextran at 4°C for 5 hours prior to testing. Dextran consists of water-soluble polysaccharides and as seen from the figure 4.1 it stains the ECM while not being able to penetrate the cell membrane of chondrocytes. During the testing samples were mounted with dental cement on the sample holder. All measurements were performed within 40 hours of sacrifice. All tissues not tested immediately were stored in Dulbecco's Modified Eagle's Medium (DMEM, Sigma Aldrich, USA) at 4 °C until the time of testing.

The measurement locations include lateral and medial condyles of femur, lateral and medial tibial plateaus, patellofemoral groove and patella. Tibial plateaus were removed from tibia and cut into ∼6x4 mm blocks, in order to mount them on the CLSM. The loaded sites are presented in figure 4.3.

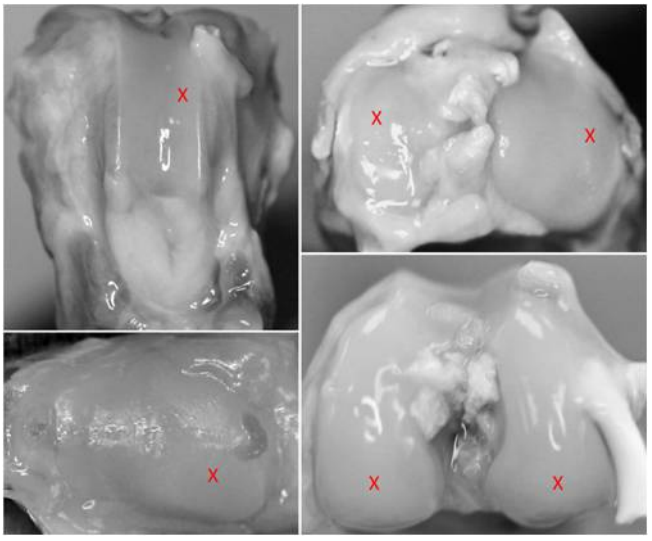

Figure 4.3: The measurement locations. Top-left patellofemoral groove, top-right tibial plateaus, bottom-left patella and bottom right femoral condyles.

Patellae were loaded on the lateral aspect, midway between the proximal and distal poles; groove tissues were loaded midway between the proximal and distal ends.

Condyles were loaded on their summits and loading on the lateral and medial plateaus was applied to an area that was shifted 1 mm laterally from the block center. Preconditioning was performed to ensure a good contact with indenter and cartilage (0.1-0.2 MPa). Then images were acquired and after that a pressure of 2 MPa was applied at an average speed of 10 µm/s. Then displacement was held constant for 20 minutes. After this, the equilibrium state was reached and the image stacks were acquired with 0.5 µm z-axis (tissue depth) increments up to 60 µm. The system was calibrated with microspheres of known diameter. The microspheres were embedded in 2% agarose gel and imaged. Apparent heights of the microspheres were determined by applying optimal thresholding method for each microsphere and its background [13]. Correction factor for z-direction distortion was obtained by dividing the known microsphere height by the average apparent height of microspheres [13].

4.2.1 Evaluation of chondrocyte morphology and local tissue properties

For every sample in the knee joints, the sample was imaged and imaging was performed before and after indentation. For every location, 10 random chondrocytes were chosen and the same cells were analyzed from before and after compression images. The cells were cropped from the 2D stacks (x-y plane size 512 x 512 pixels, pixel size 0.41 µm x 0.41 µm) and turned to grayscale images using ImageJ (National Institute of Health, USA). Thresholds between chondrocytes and background for the 3D image construction were defined similar to Han *et al.*, 2009 [13]. Briefly, for each individual chondrocyte the middle slice of the chondrocyte in z-direction was chosen for image histogram analysis. The slices were imported to MatLab (MathWorks Inc.) and thresholds were defined using median of the chondrocyte and its background [13]. The reconstruction of chondrocytes was done with custom-written Python code that used VTK 5.2.0 (the Visualized toolkit: Kitware Inc.). An example of image stacks and 3D reconstruction of cropped chondrocytes and the orientation of the xyz-coordinate system related to the chondrocyte can be seen in figure 4.1.

With the same Python script, the cropped cell images were first smoothed with gaussian function, which is effectively a low pass filtering to get rid of the high frequency image noise. Then the calculated threshold is applied and 3D object

is built using triangular polygon mesh [14]. The VTK calculates cell volume and surface area, but other dimensions of the cell, such as height and width, were calculated separately using MatLab. Used algorithm for calculating the cell dimensions is presented in appendix A.

Furthermore, global strain, local axial and transverse strains were calculated from the images. In the case of these site-specific cartilage experiments, the axial direction is parallel to tissue depth, and the transverse plane is orthogonal to the axial direction. So the axial direction is the z-axis and the transverse plane is the xy-plane. First the z-distance between cell pairs in unloaded (l_0) and loaded (l) tissue are measured. The axial ECM strain is then calculated as:

$$\epsilon_{\text{axial}} = \frac{l_0 - l}{l_0}. \tag{4.1}$$

To calculate the transverse ECM strains ($\epsilon_{transverse}$), four marker cells were tracked in xy-plane and then a strain tensor $[\epsilon]_{2\times2}$ was computed. The matrix was further diagonalized, so that the higher and lower eigenvalues represent the major and minor strains. The global strain ϵ_{global} is calculated as:

$$\epsilon_{\text{global}} = \frac{\Delta H}{H}, \tag{4.2}$$

where ΔH and H are change in tissue thickness and undeformed tissue thickness, respectively.

4.3 Biomechanical testing

Biomechanical testing was performed on different rabbit samples, but on the same six different locations of the rabbit knee joint as with CLSM. The rabbit joints were cut into four different pieces, which were patella, groove, femoral condyles and tibial plateaus. First of all, the thickness of every sample was determined using pulse-echo ultrasound. This technique based on the fact, that cartilage generates two distinguishable echoes from the surface of the cartilage and from the cartilage-bone interface [48]. From the echoes it was possible to measure the ultrasound pulse time-of-flight (t_{tof}) in cartilage. Further, the thickness of cartilage (h) was calculated with equation

$$h = \frac{1}{2} v_{\text{us}} t_{\text{tof}}, \tag{4.3}$$

where the speed of ultrasound in cartilage was approximated to be $v_{\mathrm{us}} = 1627\,\frac{\mathrm{m}}{\mathrm{s}}$. After thickness calculation the biomechanical testing routine was carried out.

The testing protocol started with lowering the indenter to contact with the sample and then a precondition was performed. This was carried out with slow strain rate of approximately 2% of the sample thickness. After ensuring the contact with the indenter and the sample (load of $\sim$ 5g), stress-relaxation test in 3 steps was carried out as shown in figure 4.4. Indentation displacement was 5% of the remaining thickness at all steps and the corresponding strain rate was 100% of the remaining thickness. The instantaneous displacement of indenter results in a sharp peak rise in stress followed by stress-relaxation, which finally leads to the stress equilibrium. A gap of 15 minutes was kept between each step, to make sure equilibrium stress had been reached before the next indentation. After stress-relaxation tests, a dynamic test was performed with four cycles at 1 Hz as shown in figure 4.4. Amplitude of the dynamic cycling was 2% of the remaining cartilage thickness.

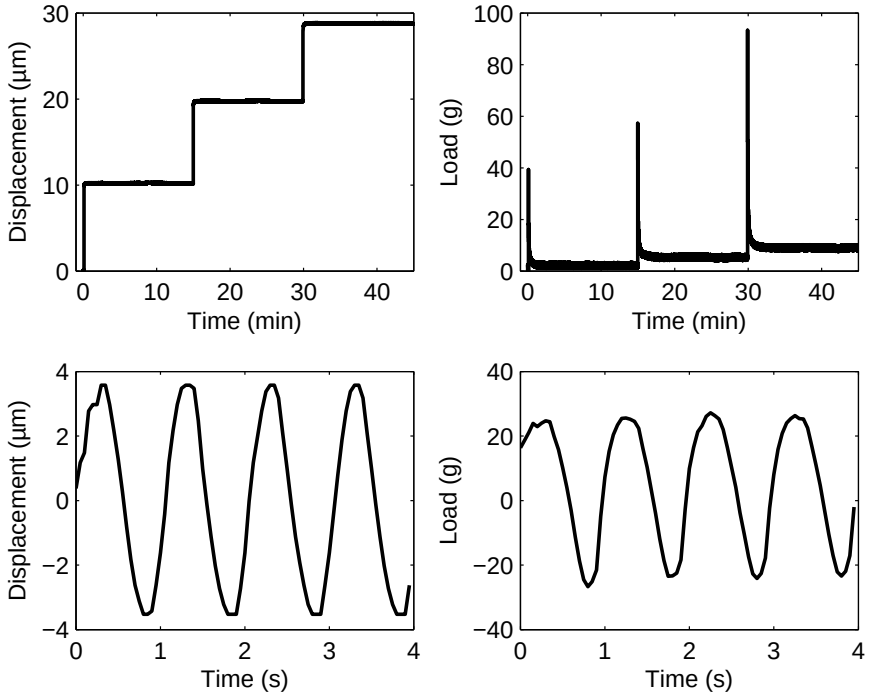

Figure 4.4: Example of dynamic stress-relaxation measurements. Top: the 3 steps of stress-relaxation measurement and the observed load. Bottom: the four cycles of dynamic loading and observed load, where load offset is applied to make the load oscillate around zero.

Sample surfaces were kept moist with phosphate buffered saline (PBS) during the sample preparation, ultrasound measurements and were also immersed in the PBS solution during the indentation tests to ensure appropriate tissue hydration.

The information about the indentation force and displacement of the intender was recorded through the use of a motion controller (Newport PM500-C Precision Motion Controller), which controls the indenter movement (radius $r = 0.5$ mm), and a load sensing unit (RDP transducer Indicator E308), which allowed real-time tracking and recording of the applied load.

Equilibrium modulus was calculated for each sample using the method described in section 2.3.2. Values used to determine moduli were $\nu = 0.2$, $r = 0.5$ mm and κ values were interpolated from the table 2.2 provided by Zhang *et al* [63]. The values of ν were not directly measured for each site, and used value is only approximation based on previous studies [24, 53]. The values of cartilage thickness H were determined by ultrasound measurements. The dynamic moduli were also calculated as described in section 2.3.2, but with the value $\nu = 0.5$ (incompressible material).

4.4 Statistics

For chondrocyte deformations (volume, dimensional) and tissue strains (global, local axial and transverse strains) the statistics were performed as following: The normality of pooled site-specific data (Kolmogorov-Smirnov test; $p < 0.05$) was assessed, and then the percent change in both cell volume and cell dimensions (height, width and depth) due to deformation were determined for all tissue sites as [(Before-After)/Before $\times$ 100]. After this, ANOVA and Tukey Post Hoc tests were performed in order to compare differences among sites ($p < 0.05$). For both the dynamic and equilibrium moduli, and for global, local, and transverse strains, the differences among sites were also compared using ANOVA and Tukey Post Hoc test ($p < 0.05$). All results are given in the form mean $\pm$ 95% confidence intervals. The sample size N for chondrocyte volumes and dimensional parameters was $N = 80 - 100$ per site. For all the different tissue strains distances between $n = 8$ cell pairs or groups per sample were measured, leading to $N = 64$ samples per tissue site. In case of the dynamic and equilibrium modulus, the sample size was $N = 10$ for each site.

Chapter 5

Results

In this thesis the rabbit knee joint was studied in a site-specific manner, so that tissues from different contacting cartilage surfaces were used. The first part of this work was to analyze images of superficial zone chondrocytes, which were taken with the CLSM indentation system. The second part of the work included biomechanical testing of the same sites as in the first part (including thickness measurements).

5.1 Chondrocyte volumes, dimensions and changes in these due to deformation

The cell parameters (cell volume, height, depth and width) obtained from before and after loading images are presented in the tables 5.1 and 5.2.

Table 5.1: Cell parameters obtained from various sites prior to compression.

Tissue site	Measured cell parameters (mean ± 95% CI)			
	Volume µm^3	Height µm	Width µm	Depth µm
Patella	477.1 ± 33.2	6.3 ± 0.3	14.3 ± 0.4	10.4 ± 0.4
Groove	605.6 ± 28.3	5.8 ± 0.2	17.1 ± 0.5	12.3 ± 0.3
Lateral condyle	612.3 ± 28.7	6.6 ± 0.2	16.6 ± 0.5	11.3 ± 0.3
Medial condyle	532.3 ± 23.1	6.6 ± 0.2	15.5 ± 0.4	10.4 ± 0.3
Lateral plateau	533.8 ± 31.8	6.3 ± 0.2	15.7 ± 0.5	10.8 ± 0.3
Medial plateau	288.2 ± 18.5	6.1 ± 0.3	10.6 ± 0.3	8.6 ± 0.2

Table 5.2: Cell parameters obtained from various sites after compression.

Tissue site	Measured cell parameters (mean ± 95% CI)			
	Volume µm^3	Height µm	Width µm	Depth µm
Patella	422.5 ± 26.5	4.9 ± 0.2	15.5 ± 0.4	10.9 ± 0.4
Groove	557.0 ± 31.7	5.0 ± 0.2	17.8 ± 0.5	12.8 ± 0.3
Lateral condyle	534.9 ± 32.1	5.0 ± 0.2	17.8 ± 0.5	12.1 ± 0.3
Medial condyle	495.4 ± 25.1	5.0 ± 0.2	16.8 ± 0.4	11.8 ± 0.3
Lateral plateau	494.9 ± 29.1	5.5 ± 0.2	16.2 ± 0.5	11.1 ± 0.3
Medial plateau	250.4 ± 11.8	4.5 ± 0.2	11.9 ± 0.3	9.1 ± 0.2

The deformation induced site-specific chondrocyte volume changes are presented in table 5.3 and in figure 5.1. Further, the changes in cell height, width and depth are presented in table 5.4 and also in figures 5.2-5.4. The exact $p-$values indicating differences in cell volume and dimensional changes between groups are presented in appendix B in tables B.1-B.4.

The statistics related to differences in cell volume and cell dimensional changes due to deformation are as following. As shown in figures 5.1-5.4, the cells from the patella underwent bigger volume changes with larger changes in both cell width and height ($p < 0.05$), but showed no change in depth, when compared to the femoral groove tissues ($p > 0.05$). Chondrocytes from the patella also exhibited larger changes in volume, height and width when compared to the lateral plateau tissues, as shown in figures 5.1-5.3 ($p < 0.05$). Chondrocytes from the groove tissues exhibited smaller changes in volume, height and width when compared to the lateral condyle tissues, which can be observed in figures 5.1-5.3 ($p < 0.05$). Lateral condyle cells in turn underwent larger changes in cell volume caused by bigger increases in width, height and also in depth direction when compared to the cells from lateral plateau, which can be seen in figures 5.1-5.4 ($p < 0.05$). Lateral condyle cells also displayed larger deformation in cell volume and smaller deformation in cell depth when compared to cells from the medial condyle, as shown in figures 5.1 and 5.4 ($p < 0.05$). The chondrocytes from the lateral plateau exhibited a smaller change in volume and also smaller changes in all three dimensional directions when compared to chondrocytes from the medial plateau, which can be seen in figures 5.1-5.4 ($p < 0.05$). Finally, as shown in figures 5.1, 5.3 and 5.4, the medial condyle cells exhibited smaller changes in volume and width and greater changes in cell depth when compared to the volume and dimensional changes of the medial plateau cells ($p < 0.05$).

Table 5.3: Percent changes in chondrocyte volumes due to cartilage deformation across various sites within the rabbit knee.

Tissue site (# cell population)	Changes (%) in cell volume due to deformation (mean ± 95% confidence intervals)
Patella (N=100)	-11.8 ± 2.4
Groove (N=90)	-7.7 ± 1.6
Lateral condyle (N=100)	-12.3 ± 2.1
Medial condyle (N=100)	-6.4 ± 2.2
Lateral plateau(N=100)	-7.0 ± 1.4
Medial plateau (N=80)	-11.8 ± 2.4

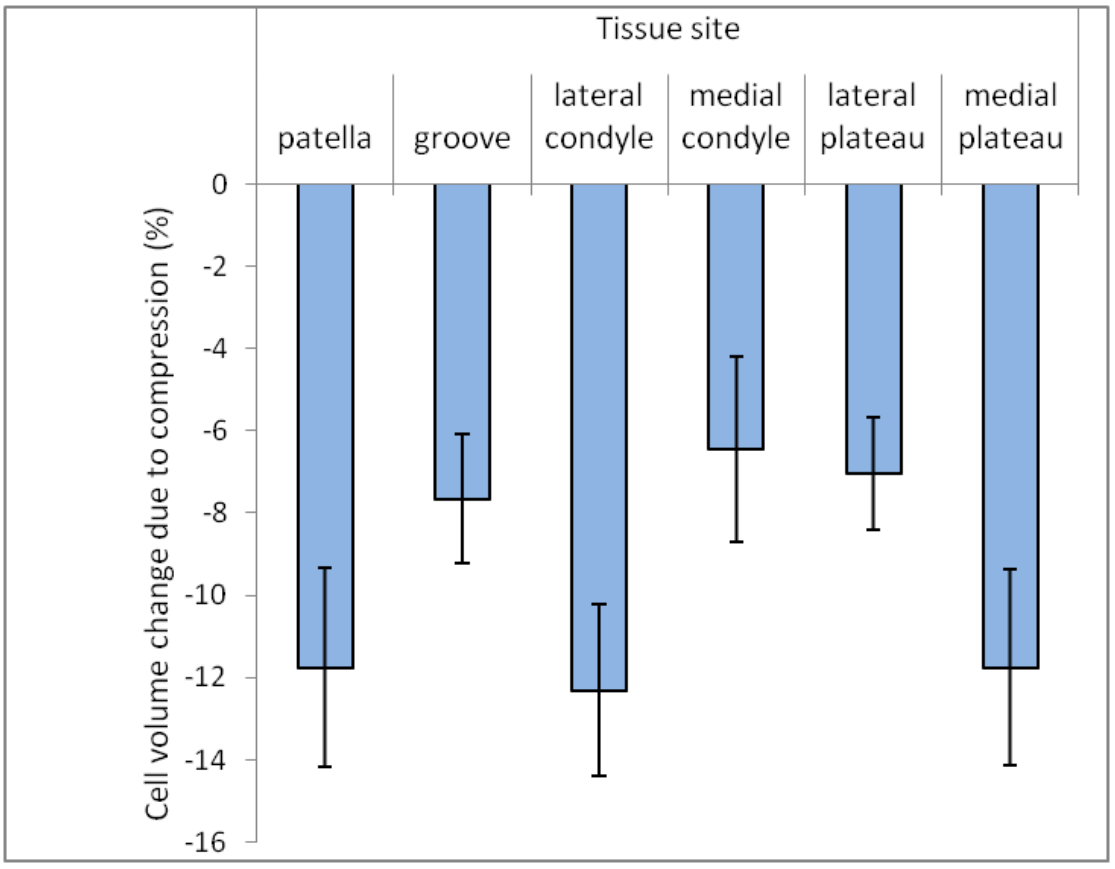

Figure 5.1: Site-specific chondrocyte volume changes due to deformation. Black bars indicate 95% confidence intervals.

Table 5.4: Percent changes in chondrocyte height, width and depth dimensions due to cartilage deformation across various sites within the rabbit knee.

Tissue site (# cell population)	Changes (%) in cell dimensions due to deformation (mean ± 95% confidence intervals)		
	Height	Width	Depth
Patella (N=100)	-20.2 ± 3.8	9.2 ± 2.3	4.9 ± 2.6
Groove (N=90)	-14.3 ± 1.7	4.1 ± 0.9	4.8 ± 1.0
Lateral Condyle (N=100)	-22.9 ± 2.1	7.2 ± 1.3	7.8 ± 1.3
Medial Condyle (N=100)	-23.1 ± 2.4	8.8 ± 1.5	14.2 ± 2.0
Lateral Plateau (N=100)	-12.5 ± 1.8	3.7 ± 0.9	3.5 ± 1.3
Medial Plateau (N=80)	-24.9 ± 2.8	12.4 ± 2.4	7.1 ± 2.6

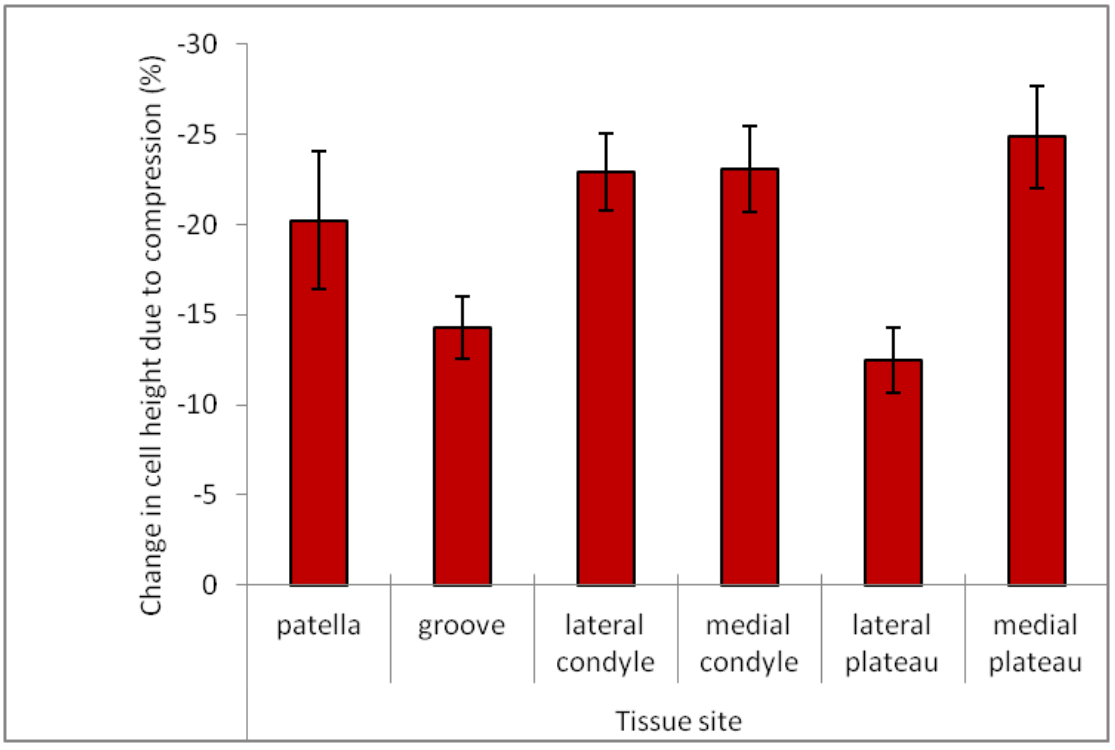

Figure 5.2: Site-specific chondrocyte height changes due to deformation. Black bars indicate 95% confidence intervals.

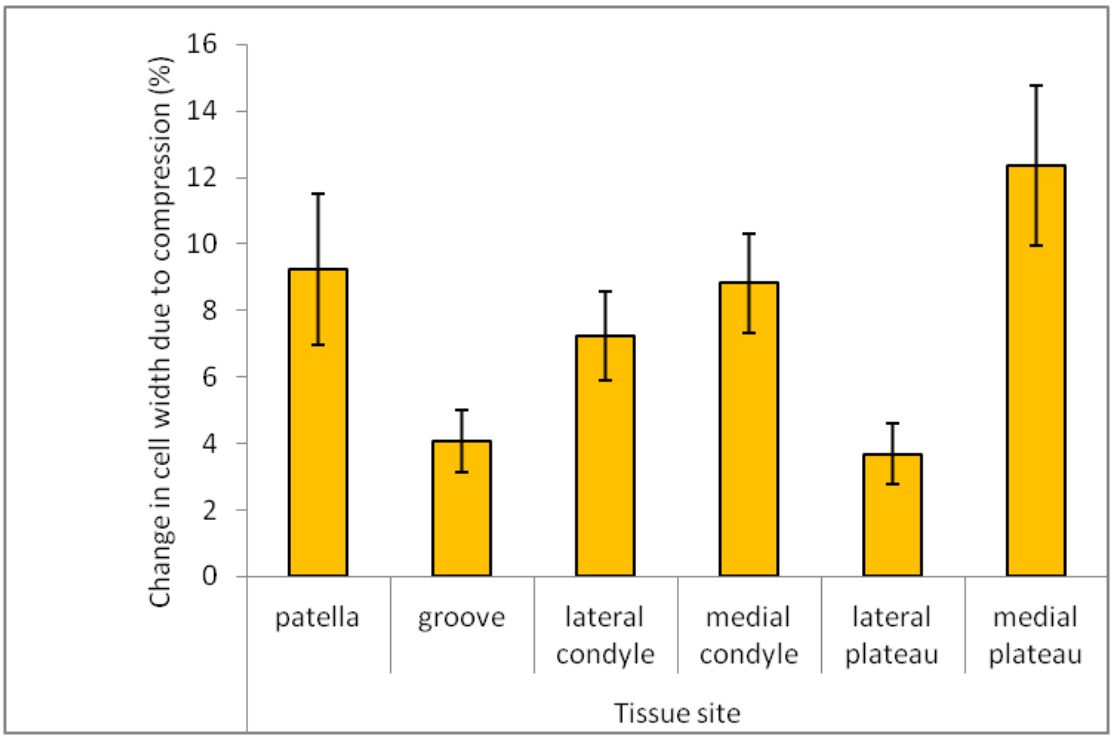

Figure 5.3: Site-specific chondrocyte width changes due to deformation. Black bars indicate 95% confidence intervals.

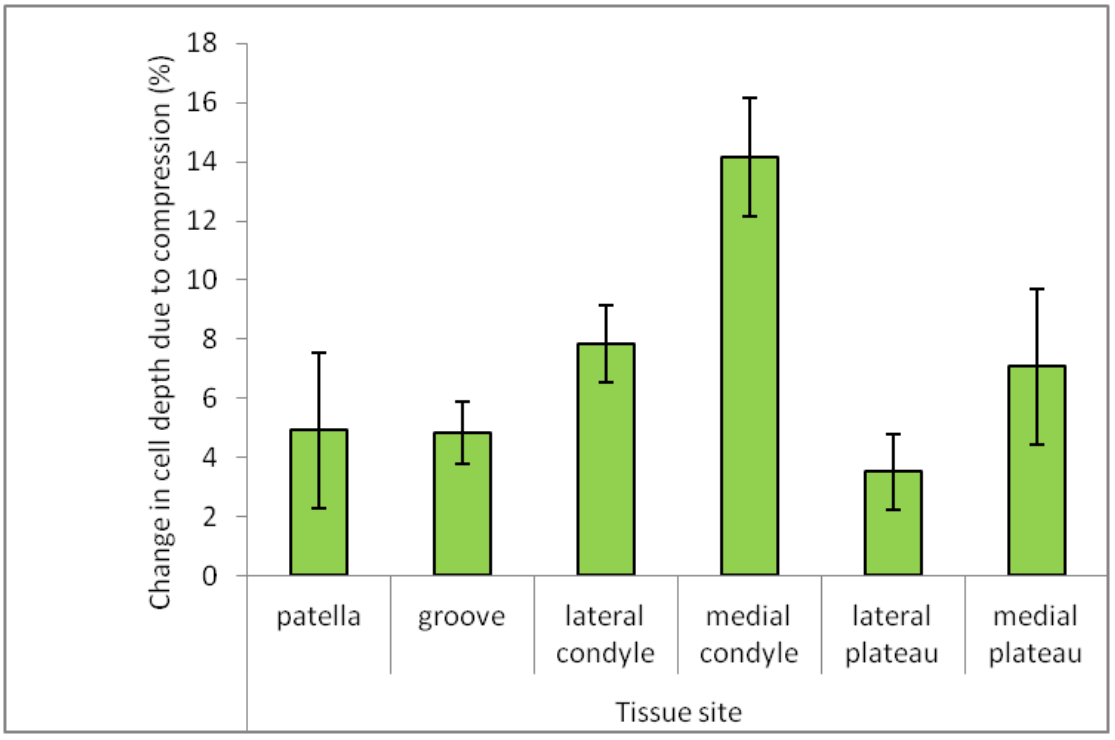

Figure 5.4: Site-specific chondrocyte depth changes due to deformation. Black bars indicate 95% confidence intervals.

5.2 Global, local axial and transverse tissue strains

Global strain, local axial and transverse strains were determined. Global strains and local axial ECM strains are presented in table 5.5 and in figure 5.5. The exact $p-$values indicating the differences between sites for these parameters are presented in appendix B in tables B.5 and B.6. Briefly the statistical differences were as following. As shown in figure 5.5, for patella tissue both the global and local strains were bigger than in groove and lateral plateau tissues, and at the same time lower than in medial condyle and medial plateau tissues ($p < 0.05$). In groove tissue, the global strain values were significantly different when compared to any other location, and local axial strain values were different for other locations except lateral plateau, which can be seen in figure 5.5 ($p < 0.05$). The lateral condyle tissues and also medial condyle tissues experienced greater global and local axial strains when compared to lateral plateau tissues, as shown in figure 5.5 ($p < 0.05$). Finally, as shown in figure 5.5, the lateral plateau tissues underwent lower strains when compared to any other location ($p < 0.05$).

Table 5.5: Global and local axial strains in different tissue sites. Data presented in form of mean ± 95% confidence intervals.

Tissue site	Global strain (%)	Local strain (%)
Patella	18.3 ± 2.0	29.7 ± 2.2
Groove	13.8 ± 2.1	22.7 ± 1.9
Lateral condyle	20.7 ± 1.6	32.1 ± 2.3
Medial condyle	22.2 ± 1.9	34.2 ± 2.3
Lateral plateau	9.8 ± 1.0	20.7 ± 1.5
Medial plateau	22.4 ± 2.0	35.0 ± 2.3

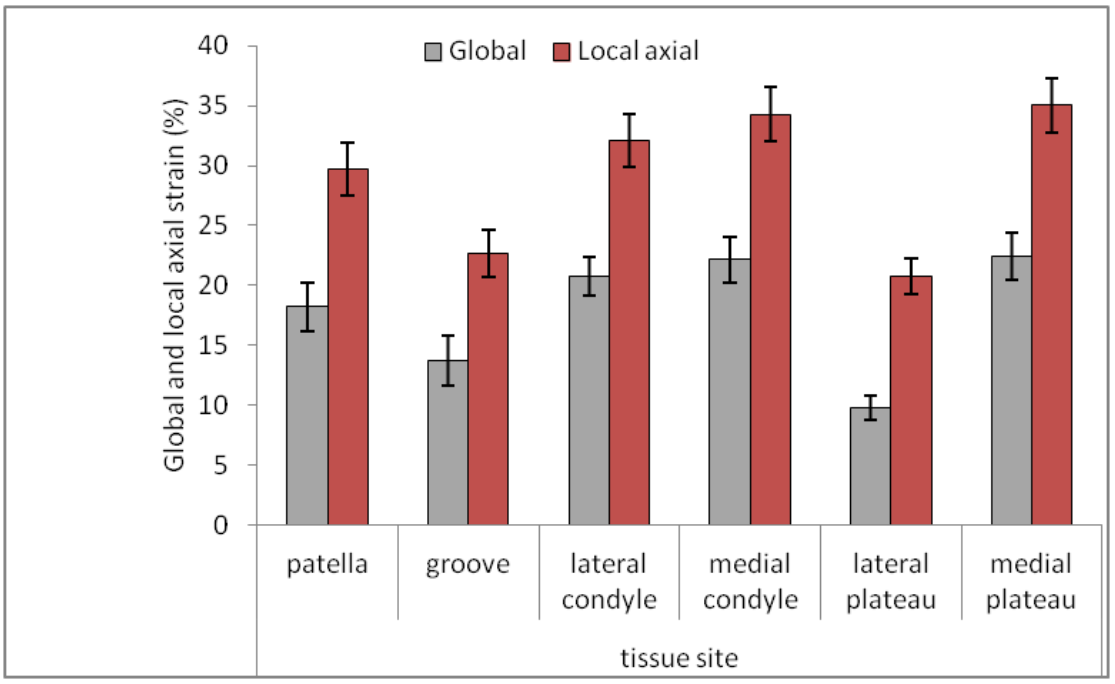

Figure 5.5: Site-specific global and local axial strain values. Black bars indicate 95% confidence intervals.

The transverse strains in minor and major direction are presented in table 5.6 and in figure 5.6. The exact $p-$values indicating the differences between sites for these parameters are presented in appendix B in tables B.7 and B.8. As shown in figure 5.6, the major direction strains in patella tissues were higher than in groove, lateral condyle and lateral plateau tissues ($p < 0.05$). For the major transverse direction, strains in groove tissues were significantly lower than in lateral condyle, medial condyle and medial plateau tissues, which can be seen in figure 5.6 ($p < 0.05$). In lateral condyle tissues the major transverse direction strains were lower than in medial condyle and medial plateau, as shown in figure 5.6 ($p < 0.05$). The major transverse direction strains in medial condyle were also higher than in lateral plateau, which can be seen in figure 5.6 ($p < 0.05$). Finally, as shown in figure 5.6, the major direction transverse strains in lateral plateau were significantly lower than those of medial plateau ($p < 0.05$).

From figure 5.6 it can be seen, that the minor transverse direction strains in patella tissues were significantly lower than in lateral condyle, medial condyle and medial plateau tissues ($p < 0.05$). The groove tissues had lower minor transverse direction strain values than the medial condyle and medial plateau tissues, as shown in figure 5.6 ($p < 0.05$). Lateral condyle tissues had higher minor transverse direction strains than those of lateral plateau tissues, which can also be seen in

5.6 ($p < 0.05$). From figure 5.6 it can be observed, that the medial condyle tissues also had significantly higher minor transverse direction strains than lateral plateau tissues ($p < 0.05$). Finally, as shown in figure 5.6, the lateral plateau tissues had lower minor transverse direction strains than the medial plateau tissues ($p < 0.05$).

Table 5.6: Major and minor transverse strains in different tissue sites. Data presented in form of mean ± 95% confidence intervals.

Tissue site	Major strain (%)	Minor strain (%)
Patella	10.0 ± 1.2	2.7 ± 1.0
Groove	4.7 ± 0.8	2.9 ± 0.6
Lateral condyle	7.1 ± 1.4	4.9 ± 1.3
Medial condyle	9.9 ± 1.1	6.1 ± 0.9
Lateral plateau	5.1 ± 0.8	2.6 ± 0.7
Medial plateau	10.9 ± 1.0	5.9 ± 0.9

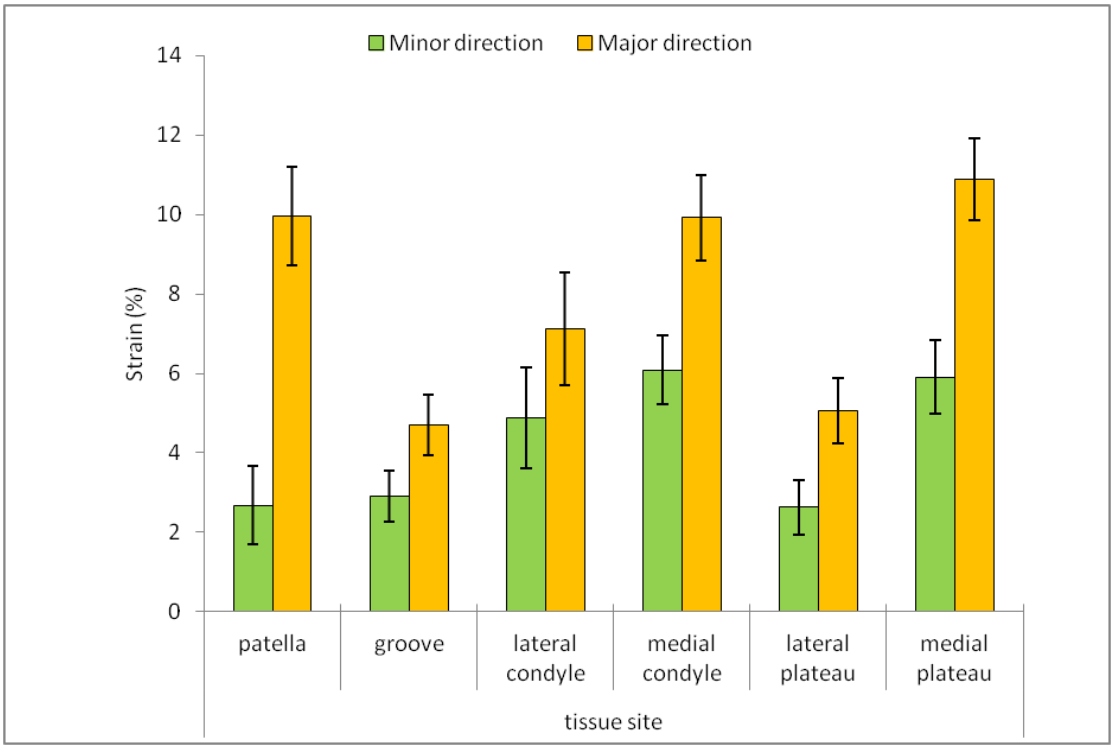

Figure 5.6: Site-specific transverse strain values in major and minor direction. Black bars indicate 95% confidence intervals.

5.3 Mechanical moduli of cartilage sites

The site-specific means of calculated equilibrium moduli are presented in table 5.7 and in figure 5.7. The calculated dynamic moduli are presented in table 5.8 and

in figure 5.8. The exact $p-$values indicating the differences between sites for these parameters are presented in appendix B in tables B.9 and B.10. The patellas' equilibrium moduli were significantly lower when compared to groove, lateral plateau and medial condyle tissues ($p < 0.05$). Furthermore, the lateral condyle tissues had significantly lower equilibrium moduli, when compared to lateral plateau and medial condyle tissues ($p < 0.05$). In case of dynamic moduli, the patella tissues had significantly lower moduli when compared to groove tissues ($p < 0.05$) and the groove tissues had significantly higher moduli when compared to medial plateau tissues ($p < 0.05$).

Table 5.7: Equilibrium modulus of different sites. Data presented in form of mean ± 95% confidence intervals.

Tissue site ($N = 10$/site)	Equilibrium modulus E (MPa)
Patella	0.2 ± 0.1
Groove	0.5 ± 0.2
Lateral condyle	0.3 ± 0.1
Medial condyle	0.6 ± 0.1
Lateral plateau	0.57 ± 0.1
Medial plateau	0.4 ± 0.2

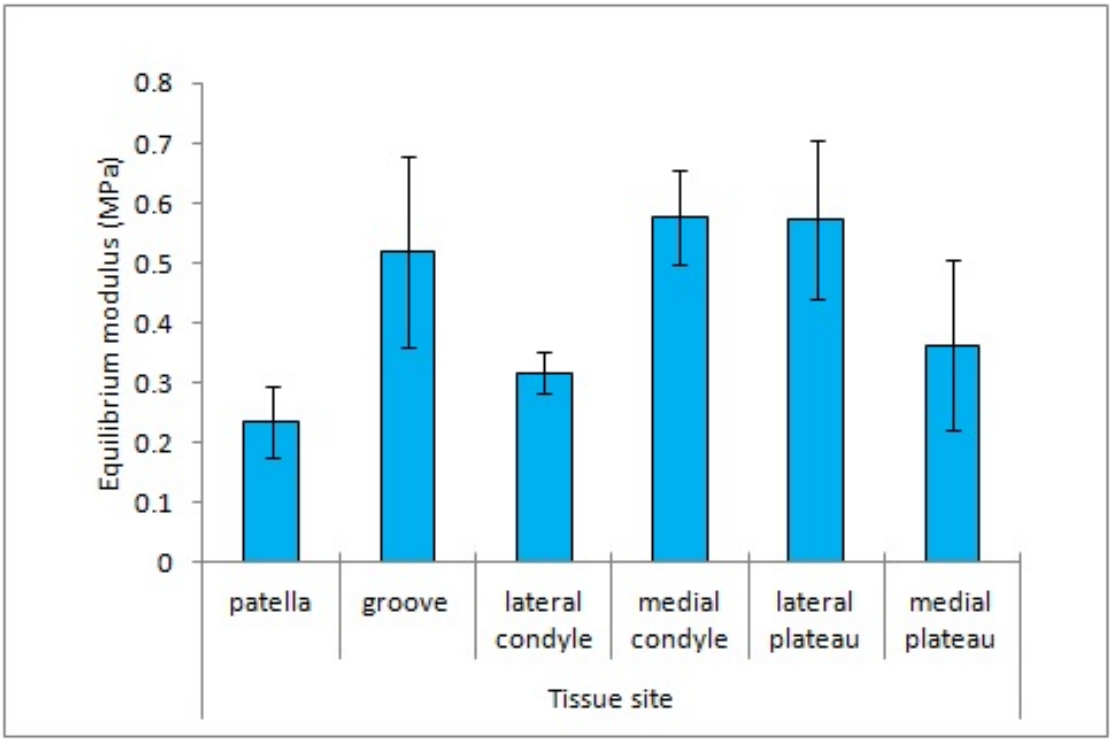

Figure 5.7: Site-specific equilibrium modulus values. Black bars indicate 95% confidence intervals.

Table 5.8: Dynamic modulus of different sites for 1 Hz indentation. Data presented in form of mean ± 95% confidence intervals.

Tissue site ($N = 10$/site)	Dynamic modulus E_{dyn} (MPa)
Patella	1.9 ± 1.0
Groove	3.6 ± 1.1
Lateral condyle	2.6 ± 0.4
Medial condyle	3.1 ± 0.8
Lateral plateau	2.9 ± 0.5
Medial plateau	1.6 ± 0.3

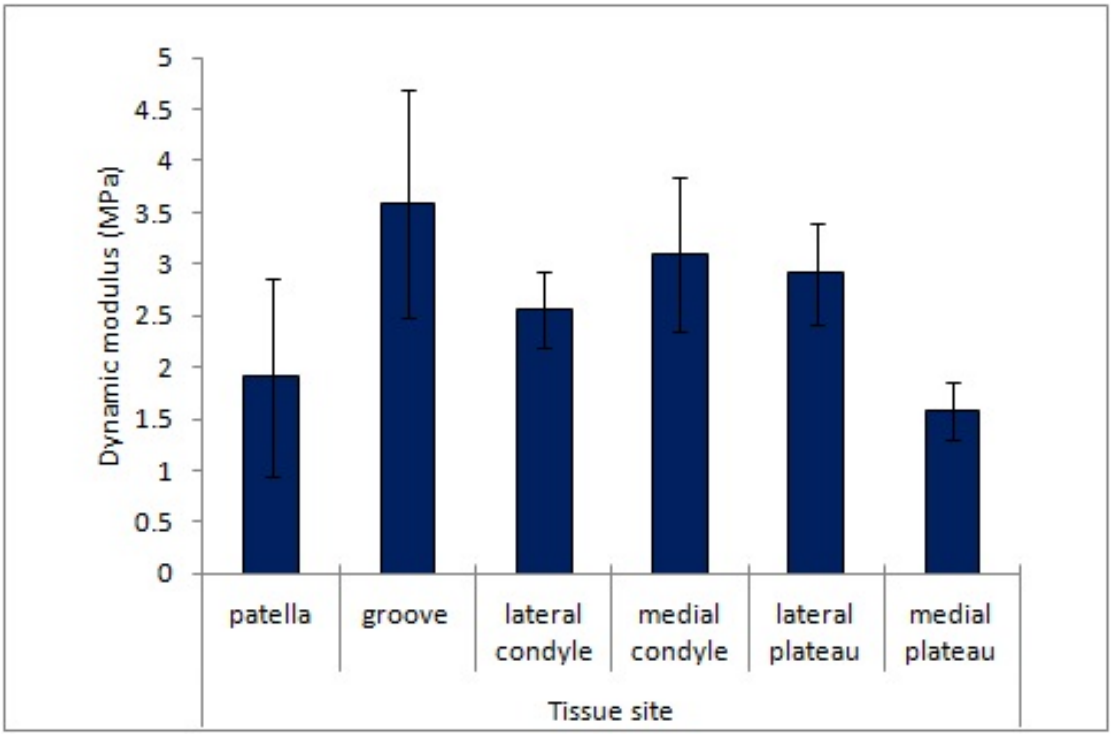

Figure 5.8: Site-specific dynamic modulus values. Black bars indicate 95% confidence intervals.

Chapter 6

Discussion

From the results, it is evident that there are site-dependent differences in chondrocyte deformation behavior and in tissue (global and both local axial and transverse) strains experienced within the rabbit knee joint. Overall, for all tissues the cell height and volume were decreasing due to compression and at the same time cell width and depth were increasing, which is as hypothesized. The global strain values were less than local axial strains at all the tissue sites, consistent with Han *et al.* (2010) [28]. The global strains are less than local axial strains, because the local strains were determined from the superficial zones of articular cartilage samples, and this zone is known to be softer than deeper tissue zones. In general, the elastic moduli seem to be inversely related to cell volume changes, meaning that if cells from specific site underwent bigger changes in cell volume when compared to other sites, the site also has lower elastic modulus than other sites. Because there are six sites and comparing them to each other is not possibly the best way to explain and present the differences, a pair-wise comparison of assumed contacting surface sites will be discussed for clarity.

When compared to groove tissues, the patella tissues underwent bigger changes in cell volume, height and width ($p < 0.05$), but the change in cell depth direction was approximately the same between the two. The bigger decrease of cell volume in patella tissues was caused by bigger decrease in cell height, which was not compensated by expansion in cell depth direction. The global and local axial strain values were bigger in patella ($p < 0.05$) and are consistent with the larger cell height deformations and lower moduli observed in the tested sites from the patella.

The transverse strains were consistent with the cell width and depth changes. Major transverse strains were significantly higher in patella tissues ($p < 0.05$), like the cell width changes, which implicates that larger strains in this direction caused the greater cell width changes. The elastic and dynamic moduli of patella were also lower than in groove ($p < 0.05$), which implies that groove is stiffer overall, and hence the tissue and the cells deform less during compression.

For the lateral condyle and plateau, the volume and height decreases in the condyle tissues were greater than in plateau tissues ($p < 0.05$). Moreover, the width and depth expansion of cells was greater in condyle tissues compared to plateau tissues ($p < 0.05$). Global and local axial strains were greater in condyle tissues. The transverse strains were consistent with cell depth and width changes and were higher in condyle tissues in both major and minor directions ($p < 0.05$). The elastic moduli were consistent with the dimension and strain differences. Dynamic response between the two sites did not show significant differences. As with the patella and groove tissues, it seems that changes in cell height are the primary factor that creates the changes in cell volume between lateral condyle and plateau.

For medial condyle and medial plateau, the volume and cell height decreases in plateau tissues were greater than in condyle ($p < 0.05$). In addition to this, the plateau cells underwent larger changes in the width direction, but smaller changes in the depth direction compared to condyle cells ($p < 0.05$). Overall the greater volume decrease of medial plateau cells was due to a smaller amount of stretching in the depth direction and greater amount of compression in the height direction. The major and minor transverse strains were similar between the sites, because the major strain measured in the plateau tissues is likely driving cell width changes, while for the condyle tissues it is causing cell depth changes, and the minor transverse strain is responsible for the cell depth changes in the plateau tissues and causes the cell width changes in the condyle tissues.

Overall, the cell-level parameter changes in cell volume and dimensions were found to be related to the tissue-level parameters such as tissue strains and equilibrium moduli. The cell expansion is anisotropic at all tissue sites, implying that the local collagen structure is affecting the cell expansion in lateral directions. Moreover, the differences in major and minor tissue transverse strains are consistent with the anisotropic lateral expansion of the chondrocytes. The height changes of the chondrocytes are in comparison clearly linked to the local axial and global tissue strain as well as inversely proportional to the equilibrium moduli of the samples.

There have been other studies about how mechanical loading affects chondrocytes. One of the early studies was performed by Guilak *et al.*, 1995. They investigated chondrocyte morphology and local tissue deformation in explants [25]. The findings were that cell volume and height were decreasing in superficial, middle and the deep zones due to compression, but significantly more in the superficial zone. Also it was observed that in the superficial zone a significant lateral expansion occurred in the direction perpendicular to the local split-line pattern [25]. Compared to this thesis the cell volume decrease they observed was 22% for the superficial zone chondrocytes, which is considerably higher than changes observed in this thesis. This could be due to fact that the samples used were explants and they were imaged from the side of the articular cartilage and not from the top like in our case.

In study of lapine retropatellar cartilage after ACLT (Han *et al.* 2010), the ACLT group (9 weeks) showed changes in chondrocyte deformations compared to the contralateral and control group [28]. In their study, the deformations were identical between groups to depth and height directions, but ACLT group chondrocytes deformed $12 \pm 1\%$ in width direction compared to control and contralateral deformation of $6 \pm 1\%$. Also they saw a volume increase of $8 \pm 3\%$ in early OA tissue and decrease of $-8 \pm 1\%$ for other groups [28]. For comparison, the values of cell height change, local tissue strain, major and minor transverse strain and change in cell volume are compared between the current study and their study. The values of both studies are shown in figure 6.1, from which it can be observed that the values were consistent for the patella tissues between the studies. However, the most important part is that their study indicates that cell behaviour is altered in traumatized joint. This indicates that cell response is altered when the dynamics of the joint are disturbed.

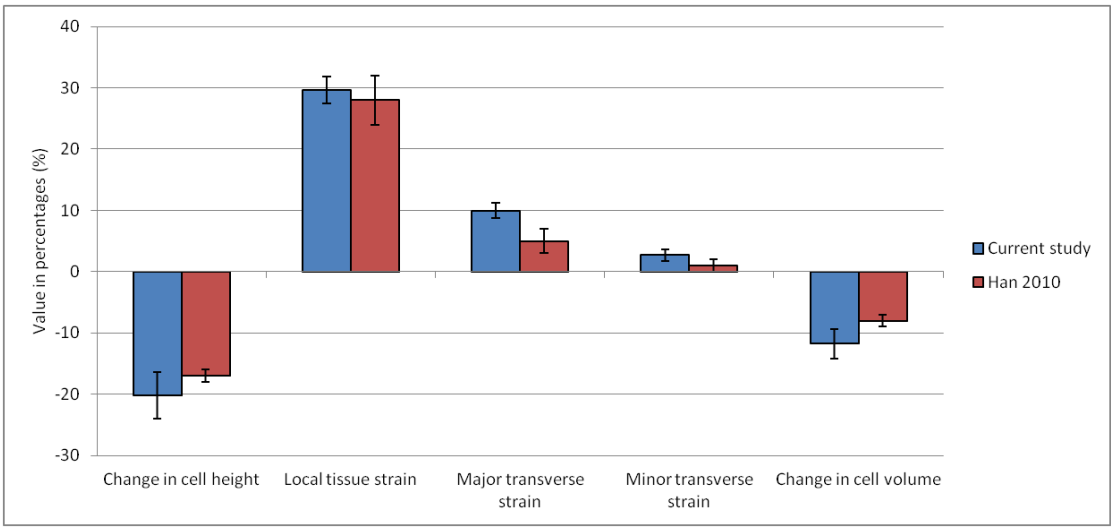

Figure 6.1: Various values for the patella tissues from the current study and corresponding values from study by Han *et al.*, 2010 [28].

In a study of chondrocyte deformation under extreme tissue strain (Madden *et al.* 2013), it was noticed that at low loads the ECM strains in the superficial zone is higher than applied strain, but at extreme loads the local ECM strains is smaller than applied strain [20]. This implies that the local ECM and PCM environment is protecting chondrocytes from potentially damaging strains at high loads. In this study, they also saw a difference in mechanical response of cells taken from femoral condyles and patella. Furthermore, for each site the cell response was varying as a function of the applied strain, implying that both the mechanical load and the local AC structure are affecting the cell mechanics [20].

In a study of *in situ* chondrocytes within human tibial plateau AC of varying grades of degeneration (Bush and Hall, 2003), it was observed that the increase in volume of the chondrocytes was directly dependent on the cartilage degeneration and hydration [32]. This dependency was evident in surface and middle zones but not significant in the deep zone of cartilage. Tissue swelling was also greater than the increased tissue hydration caused by OA, which suggests that other factors, such as matrix metabolism, are causing the increase in chondrocyte volume [32]. For our study, this implies that metabolic differences between the sites likely cause the differences in cell response. The metabolic differences may possibly arise from different loading patterns or structural properties of the cartilage [32].

If the equilibrium moduli and dynamic moduli that were measured in our study are compared to those reported in study by Mäkelä *et al.* [76], the site-dependent differences were consistent. In both studies the mean equilibrium and mean dynamic

modulus of medial plateau tissues is lower than in lateral plateau tissues and the mean moduli of lateral condyle tissues are lower than in medial condyle tissues. In their study the groove tissues had lower equilibrium and dynamic moduli values compared to the femoral condyle or tibial plateau tissues, which were similar with the groove tissue's moduli in the current study. However, the differences between medial and lateral compartments of the femoral condyles and the tibial plataeus were evident in the both studies, which means that the tissue stiffness is likely affected by the different loads experienced at these tissue sites during the joint movement.

Overall, the dynamic and equilibrium moduli were consistently greater at the tissue sites, where the cells underwent lower volume and height changes due to deformation. The relation between these parameters was observed, even though the moduli values give global tissue response, whereas the cell volume and height changes are restricted to the local properties in the surface layer of the AC. Because chondrocytes can remodel the ECM structure, it is possible that differences between the tissue sites arise from different functional requirements of the joint tissues, which drive the cell biosynthesis and mechanical tissue properties.

Chapter 7

Conclusions

The results of this study show that:

1. There are differences in the mechanical properties of tissue and in the deformation responses of chondrocytes between the varying sites of the rabbit knee joint.
2. The volume decreases of chondrocytes due to deformation were driven by cell height decreases, which were always considerably larger than cell expansion in lateral directions.
3. Anistropic cell deformation in lateral directions implies that local tissue structure causes the cells to deform in a preferred way, which is consistent with observed tissue strains.
4. The mechanical moduli of cartilage were observed to be inversely proportional to the cell height changes, implying that stiffness of the tissue affects the cell height changes.

In more detail, the equilibrium modulus of tissue tells about the stiffness of the matrix, because at equilibrium the stress is totally carried by the ECM and fluid flow in AC is minimal. It was observed that equilibrium moduli were inversely proportional to the cell height changes, which further implies that the tissue structure is driving the mechanical response of chondrocytes. The dynamic modulus may not be compared to the cell data because morphology changes were measured at equilibrium. However, it is observed that dynamic moduli vary among the different sites studied, and this is important because the dynamic response is mainly

determined by the collagen network integrity. These observations are consistent with the fact that dynamic and equilibrium moduli vary among the knee joint sites [76].

As hypothesized the results imply that the mechanical response of the chondrocytes is dependent on the local tissue compression, which means that the local cell and tissue structure are driving the cells to deform in preferred way. It was also seen that the cell level deformation was driven by the mechanical loads, because cell height decreases were always considerably larger than cell expansion in the lateral directions. In conclusion, it seems that mechanobiological response of chondrocytes to deformation is driven by both the tissue composition and the external mechanical forces.

Overall, this study gives solid reference values for future studies about deformation-induced cell morphology changes within the rabbit knee joint. Possible applications could be engineered cell constructs, induced OA studies or even endoprosthesis materials. More precisely, the values given in this study can be compared to see if the engineered cells respond as native cells, or if induced OA changes the cell behaviour at some specific locations, or if metal-cartilage contacts alter the cell behaviour when compressed (relative to a cartilage-on-cartilage contact).

The significance of this study to mechanobiology of the chondrocytes is that the ECM and PCM properties are at least partly controlling the mechanical response of the chondrocytes to the tissue deformation, as shown by the connection between tissue strains and cell dimensional changes. Further, because the ECM and PCM structure is modeled by the chondrocytes, this implies that the chondrocytes may actually control their deformation to some point by controlling the surrounding PCM and ECM structure and composition. The inherent different functional requirements of joint sites and the varying forces experienced in these sites may drive the chondrocytes to model the local structure to withstand the lower or higher loading patterns.

Chapter 8

Current limitations, challenges and future studies

The main limitation with the CLSM technique is the maximum depth that can be imaged. For AC this means that only superficial zone chondrocytes or at maximum chondrocytes from the upper middle zone can be studied. For the cell volume and dimension analysis, the sample size was large enough and moreover the photobleaching errors should be less than 5% as reported by Moo *et al.*, 2013 [66]. To explain the transverse strains and lateral expansion of cells, which were clearly direction dependent, the local split-line pattern of the samples should have been determined. There was also a problem with the Dextran not dyeing some samples well enough. This happened for one knee's groove tissue and for two knees' medial plateau tissues. These samples were excluded from cell morphology and tissue strain analyses.

For dynamic and elastic moduli the sample size of 10 per site could have been bigger. Also in dynamical testing a porous intender might give better results by enabling higher fluid flow out of the cartilage and hence model the cartilage-on-cartilage situation better. The thickness values determined by the ultrasound may not be as accurate as values determined from, for example histological sections. If more accurate values of thicknesses become available in future, the moduli values could be corrected accordingly. Also the moduli reflect global tissue response across all the zones of AC, whereas the cell deformations and local strains are from the surface zone and the other zones could not be studied.

The samples were to be imaged with CLSM as fast as possible after sacrificing the animals, but because the imaging was a slow procedure the last samples were imaged close to 40 hours after the sacrifice. This however should not be a big problem, due to fact samples were stored in DMEM at 4°C until the measurements, which should preserve the biological state of the samples well beyond 40 hours [20]. The main challenge with the samples was with tibial plateaus (which had to be cut into blocks before imaging) and the femoral groove (which had to be cut from the femoral condyles before imaging).

Future studies will investigate tissue composition and structural properties of these tissues to determine if site-specific differences exist. This information would aid in explaining what causes the differences in cell morphology. The driving factor could be for example collagen orientation or PG content as seen with ACLT studies of the rabbit knee joint [24, 76]. Furthermore, investigations will be performed to explore if a surgical intervention such as a partial menisectomy can alter deformation-induced cell responses in the rabbit knee joint and can mimic very early changes in AC that may resemble the onset of OA.

Another possible future study would be to determine the biological response of the chondrocytes to deformation. This would provide information about how the matrix synthesis of the cells is connected to the cellular deformation or how gene expressions are linked to the nuclear deformation. Furthermore, this would provide information if the chondrocytes actually adapt the local tissue environment to deform in an optimal way for the cells.

Appendix A

Calculation of cell dimensions

The VTK provides the mesh coordinates $(x, y, z) \in \mathbb{R}^3$, which correspond to the cell's surface. The following quadric fitting algorithm was used to fit an ellipsoid to the surface coordinates and calculate lengths of the ellipsoid semi-principal axes [49]. First of all, the implicit equation for a quadric surface, like an ellipsoid or a hyperboloid, can be written as:

$$ax^2 + by^2 + cz^2 + 2dxy + 2exz + 2gyz + 2fx + 2hy + 2kz + 1 = 0, \tag{A.1}$$

which is same as:

$$f(x, y, z) = \begin{bmatrix} x & y & z & 1 \end{bmatrix} \begin{bmatrix} a & d & e & f \\ d & b & g & h \\ e & g & c & k \\ f & h & k & 1 \end{bmatrix} \begin{bmatrix} x \\ y \\ z \\ 1 \end{bmatrix} = 0, \tag{A.2}$$

where a, b, c, d, e, f, g, h and k are constants. The least squares solution will minimize the expression:

$$L = \sum_{i=1}^{N} [f(x_i, y_i, z_i)]^2. \tag{A.3}$$

Taking partial derivatives of L with respect to a, b, c, d, e, f, g, h and k and setting the derivatives to zero leads to a system of equations, which can be presented in matrix form and formally solved as:

$$\mathbf{A}\theta = \mathbf{b} \Longleftrightarrow \theta = \mathbf{A}^{-1}\mathbf{b}, \tag{A.4}$$

where:

$$\theta = \begin{bmatrix} a \\ b \\ c \\ d \\ e \\ g \\ f \\ h \\ k \end{bmatrix}, \quad \mathbf{b} = - \begin{bmatrix} \sum x_i^2 \\ \sum y_i^2 \\ \sum z_i^2 \\ \sum x_i y_i \\ \sum x_i z_i \\ \sum y_i z_i \\ \sum x_i \\ \sum y_i \\ \sum z_i \end{bmatrix}, \quad \mathbf{A} = \begin{bmatrix} \mathbf{A}_{11} & \mathbf{A}_{12} & \mathbf{A}_{13} \\ \mathbf{A}_{21} & \mathbf{A}_{22} & \mathbf{A}_{23} \\ \mathbf{A}_{31} & \mathbf{A}_{32} & \mathbf{A}_{33} \end{bmatrix}$$

$$\mathbf{A}_{11} = \begin{bmatrix} \sum x_i^4 & \sum x_i^2 y_i^2 & \sum x_i^2 z_i^2 \\ \sum x_i^2 y_i^2 & \sum y_i^4 & \sum y_i^2 z_i^2 \\ \sum x_i^2 z_i^2 & \sum y_i^2 z_i^2 & \sum z_i^4 \end{bmatrix}, \quad \mathbf{A}_{21} = \begin{bmatrix} \sum x_i^3 y_i & \sum x_i y_i^3 & \sum x_i y_i z_i^2 \\ \sum x_i^3 z_i & \sum x_i y_i^2 z_i & \sum x_i z_i^3 \\ \sum x_i^2 y_i z_i & \sum y_i^3 z_i & \sum y_i z_i^3 \end{bmatrix}$$

$$\mathbf{A}_{31} = \begin{bmatrix} \sum x_i^3 & \sum x_i y_i^2 & \sum x_i z_i^2 \\ \sum x_i^2 y_i & \sum y_i^3 & \sum y_i z_i^2 \\ \sum x_i^2 z_i & \sum y_i^2 z_i & \sum z_i^3 \end{bmatrix}, \quad \mathbf{A}_{22} = 2 \begin{bmatrix} \sum x_i^2 y_i^2 & \sum x_i^2 y_i z_i & \sum x_i y_i^2 z_i \\ \sum x_i^2 y_i z_i & \sum x_i^2 z_i^2 & \sum x_i y_i z_i^2 \\ \sum x_i y_i^2 z_i & \sum x_i y_i z_i^2 & \sum y_i^2 z_i^2 \end{bmatrix}$$

$$\mathbf{A}_{32} = 2 \begin{bmatrix} \sum x_i^2 y_i & \sum x_i^2 z_i & \sum x_i y_i z_i \\ \sum x_i y_i^2 & \sum x_i y_i z_i & \sum y_i^2 z_i \\ \sum x_i y_i z_i & \sum x_i z_i^2 & \sum y_i z_i^2 \end{bmatrix}, \quad \mathbf{A}_{33} = 2 \begin{bmatrix} \sum x_i^2 & \sum x_i y_i & \sum x_i z_i \\ \sum x_i y_i & \sum y_i^2 & \sum y_i z_i \\ \sum x_i z_i & \sum y_i z_i & \sum z_i^2 \end{bmatrix}$$

$$\mathbf{A}_{12} = 2\mathbf{A}_{21}^T, \quad \mathbf{A}_{13} = 2\mathbf{A}_{31}^T \quad \text{and} \quad \mathbf{A}_{23} = \mathbf{A}_{32}^T.$$

Once the matrix $\mathbf{A}$ is built and the quadric coefficients θ are solved, it is possible to determine the type of quadric from the properties of matrices:

$$\mathbf{D} = \begin{bmatrix} a & d & e \\ d & b & g \\ e & g & c \end{bmatrix} \quad \text{and} \quad \mathbf{E} = \begin{bmatrix} a & d & e & f \\ d & b & g & h \\ e & g & c & k \\ f & h & k & 1 \end{bmatrix}. \tag{A.5}$$

First, the eigenvalues of $\mathbf{D}$ must be calculated as:

$$\det(\mathbf{D} - \mathbf{I}\lambda) = \begin{vmatrix} a-\lambda & d & e \\ d & b-\lambda & g \\ e & g & c-\lambda \end{vmatrix} = 0. \tag{A.6}$$

Let the eigenvalues be λ_1, λ_2 and λ_3. In addition, let $p_1 = \text{rank}(\mathbf{D})$, $p_2 = \text{rank}(\mathbf{E})$, rank being the number of linearly independent columns in the matrix, and define:

$$\mu = \begin{cases} 1 & \text{if sign of the non-zero } \lambda_i\text{s is the same} \\ 0 & \text{otherwise.} \end{cases} \tag{A.7}$$

Now the type of quadric is determined according to table A.1.

Table A.1: Types of quadrics [49].

Type of surface	p_1	p_2	sign of $\det(\mathbf{E})$	μ
Real ellipsoid	3	4	-	1
Imaginary ellipsoid	3	4	+	1
Hyperboloid of one sheet	3	4	+	0
Hyperboloid of two sheets	3	4	-	0
Real quadric cone	3	3		0
Imaginary quadric cone	3	3		1
Elliptic paraboloid	2	4	-	0
Hyperbolic paraboloid	2	4	+	0
Real elliptic cylinder	2	3		1
Imaginary elliptic cylinder	2	3		1
Hyperbolic cylinder	2	3		0
Real intersecting planes	2	2		0
Imaginary intersecting planes	2	2		1
Parabolic cylinder	1	3		
Imaginary parallel planes	1	2		
Coincident planes	1	2		
Real parallel planes	1	1		

Let us next consider a real ellipsoid positioned about the origin. The equation in

body coordinates is then:

$$\frac{\hat{x}^2}{r_1^2} + \frac{\hat{y}^2}{r_2^2} + \frac{\hat{z}^2}{r_3^2} = 1, \tag{A.8}$$

which in the form of (A.2) is

$$\begin{bmatrix} \hat{x} & \hat{y} & \hat{z} & 1 \end{bmatrix} \begin{bmatrix} \frac{-1}{r_1^2} & 0 & 0 & 0 \\ 0 & \frac{-1}{r_2^2} & 0 & 0 \\ 0 & 0 & \frac{-1}{r_3^2} & 0 \\ 0 & 0 & 0 & 1 \end{bmatrix} \begin{bmatrix} \hat{x} \\ \hat{y} \\ \hat{z} \\ 1 \end{bmatrix} = 0. \tag{A.9}$$

Furthermore, the ellipsoid can be written in general coordinates after rotation and translation as:

$$\begin{bmatrix} x \\ y \\ z \end{bmatrix} = \mathbf{R} \begin{bmatrix} \hat{x} \\ \hat{y} \\ \hat{z} \end{bmatrix} + \begin{bmatrix} x_0 \\ y_0 \\ z_0 \end{bmatrix}, \tag{A.10}$$

where $\mathbf{R}$ is 3×3 rotation matrix and (x_0, y_0, z_0) is the translated position of the ellipsoid origin. Solving (A.10) for $\hat{x}, \hat{y}, \hat{z}$ and substituting into equation (A.9) yields the equation in general coordinates, which can be shown to be:

$$\begin{aligned} f(x,y,z) \;\; = & \begin{bmatrix} x & y & z & 1 \end{bmatrix} \begin{bmatrix} & & & 0 \\ & \mathbf{P} & & 0 \\ & & & 0 \\ 0 & 0 & 0 & 1 \end{bmatrix} \begin{bmatrix} x \\ y \\ z \\ 1 \end{bmatrix} - 2 \begin{bmatrix} x_0 & y_0 & z_0 \end{bmatrix} \mathbf{P} \begin{bmatrix} x \\ y \\ z \end{bmatrix} \\ & + \begin{bmatrix} x_0 & y_0 & z_0 \end{bmatrix} \mathbf{P} \begin{bmatrix} x_0 \\ y_0 \\ z_0 \end{bmatrix} + 1, \end{aligned} \tag{A.11}$$

where we have used the notation:

$$\mathbf{P} = \mathbf{R} \begin{bmatrix} \frac{-1}{r_1^2} & 0 & 0 \\ 0 & \frac{-1}{r_2^2} & 0 \\ 0 & 0 & \frac{-1}{r_3^2} \end{bmatrix} \mathbf{R}^T. \tag{A.12}$$

Equation (A.12) is actually eigendecomposition of matrix $\mathbf{P}$, which implies that eigenvectors of $\mathbf{P}$ compose the rotation matrix $\mathbf{R}$, and also the eigenvalues of $\mathbf{P}$ are inversely proportional to the ellipsoid radii squared. In addition, the last term

of equation (4.11) is constant and can be marked as:

$$C = \begin{bmatrix} x_0 & y_0 & z_0 \end{bmatrix} \mathbf{P} \begin{bmatrix} x_0 \\ y_0 \\ z_0 \end{bmatrix} + 1, \tag{A.13}$$

which leads to relation $\mathbf{D} = \frac{1}{C}\mathbf{P}$. Moreover, it can be shown that the position of ellipsoid in general coordinates is related to the parameters f, h and k of matrix $\mathbf{E}$, so that:

$$\begin{bmatrix} x_0 \\ y_0 \\ z_0 \end{bmatrix} = -\mathbf{D}^{-1} \begin{bmatrix} f \\ h \\ k \end{bmatrix}. \tag{A.14}$$

Furthermore, from equations (4.13) and (4.14) it follows that:

$$C = \left(1 + \begin{bmatrix} x_0 & y_0 & z_0 \end{bmatrix} \begin{bmatrix} f \\ h \\ k \end{bmatrix} \right)^{-1}. \tag{A.15}$$

To sum this up, the radii of the ellipsoid semi-principal axes are finally calculated as:

$$r_i = \sqrt{\frac{-1}{C\lambda_i}} \qquad i = 1, 2, 3. \tag{A.16}$$

Now, the lengths of semi-principal axes are equivalent to the width, depth and height of the cell. An example of data and fitted ellipsoid can be seen in figure A.1.

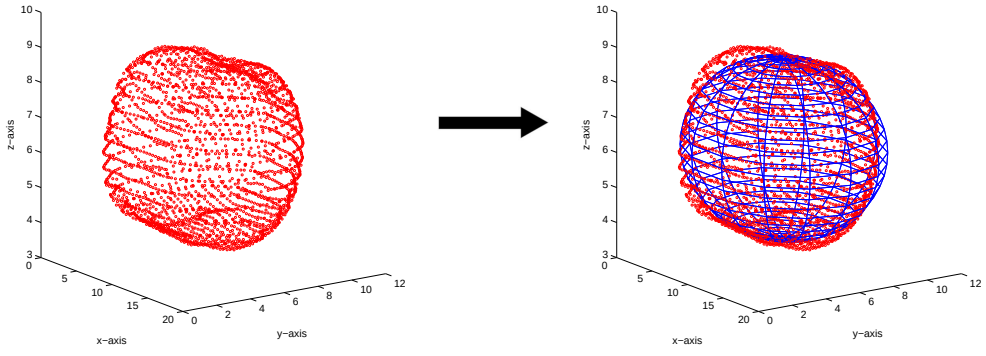

Figure A.1: Plot of cropped cell's surface (x,y,z)-coordinates and ellipsoid fitted to the coordinates.

Appendix B

Exact $p-$values

This appendix contains all the exact p-values received by statistical tests.

= p-value < 0.05.

Table B.1: The p-values corresponding to cell volume change differences between sites.

	Patella	Groove	Lat Con	Med Con	Lat Plat	Med Plat
Patella		0.060	0.999	0.003	0.013	1
Groove	0.060		0.020	0.961	0.998	0.089
Lat Con	0.999	0.020		<0.001	0.003	0.999
Med Con	0.003	0.961	<0.001		0.998	0.006
Lat Plat	0.013	0.998	0.003	0.998		0.023
Med Plat	1	0.089	0.999	0.006	0.023	

Table B.2: The p-values corresponding to cell height change differences between sites.

	Patella	Groove	Lat Con	Med Con	Lat Plat	Med Plat
Patella		0.016	0.657	0.610	< 0.001	0.143
Groove	0.016		< 0.001	< 0.001	0.926	< 0.001
Lat Con	0.657	< 0.001		1	< 0.001	0.911
Med Con	0.610	< 0.001	1		< 0.001	0.933
Lat Plat	< 0.001	0.926	< 0.001	< 0.001		< 0.001
Med Plat	0.143	< 0.001	0.911	0.933	< 0.001	

Table B.3: The p-values corresponding to cell width change differences between sites.

	Patella	Groove	Lat Con	Med Con	Lat Plat	Med Plat
Patella		< 0.001	0.499	0.999	< 0.001	0.099
Groove	< 0.001		0.077	0.001	0.999	< 0.001
Lat Con	0.499	0.077		0.730	0.023	< 0.001
Med Con	0.999	0.001	0.730		< 0.001	0.041
Lat Plat	< 0.001	0.999	0.023	< 0.001		< 0.001
Med Plat	0.099	< 0.001	< 0.001	0.041	< 0.001	

Table B.4: The p-values corresponding to cell depth change differences between sites.

	Patella	Groove	Lat Con	Med Con	Lat Plat	Med Plat
Patella		1	0.232	< 0.001	0.898	0.636
Groove	1		0.234	< 0.001	0.926	0.627
Lat Con	0.232	0.234		< 0.001	0.014	0.994
Med Con	< 0.001	< 0.001	< 0.001		< 0.001	< 0.001
Lat Plat	0.898	0.926	0.014	< 0.001		0.115
Med Plat	0.636	0.627	0.994	< 0.001	0.115	

Table B.5: The p-values corresponding to global tissue strain differences between sites.

	Patella	Groove	Lat Con	Med Con	Lat Plat	Med Plat
Patella		0.014	0.409	0.046	< 0.001	0.025
Groove	0.014		< 0.001	< 0.001	0.039	< 0.001
Lat Con	0.409	< 0.001		0.887	< 0.001	0.779
Med Con	0.046	< 0.001	0.887		< 0.001	1
Lat Plat	< 0.001	0.039	< 0.001	< 0.001		< 0.001
Med Plat	0.025	< 0.001	0.779	1	< 0.001	

Table B.6: The p-values corresponding to local axial tissue strain differences between sites.

	Patella	Groove	Lat Con	Med Con	Lat Plat	Med Plat
Patella		< 0.001	0.416	0.009	< 0.001	0.003
Groove	< 0.001		< 0.001	< 0.001	0.676	< 0.001
Lat Con	0.416	< 0.001		0.534	< 0.001	0.264
Med Con	0.009	< 0.001	0.534		< 0.001	0.264
Lat Plat	< 0.001	0.676	< 0.001	< 0.001		< 0.001
Med Plat	0.003	< 0.001	0.264	0.992	< 0.001	

Table B.7: The p-values corresponding to major transverse tissue strain differences between sites.

	Patella	Groove	Lat Con	Med Con	Lat Plat	Med Plat
Patella		< 0.001	0.007	1	< 0.001	0.868
Groove	< 0.001		0.041	< 0.001	0.998	< 0.001
Lat Con	0.007	0.041		0.008	0.1	< 0.001
Med Con	1	< 0.001	0.008		< 0.001	0.842
Lat Plat	< 0.001	0.998	0.1	< 0.001		< 0.001
Med Plat	0.868	< 0.001	< 0.001	0.842	< 0.001	

Table B.8: The p-values corresponding to minor transverse tissue strain differences between sites.

	Patella	Groove	Lat Con	Med Con	Lat Plat	Med Plat
Patella		0.999	0.019	< 0.001	1	< 0.001
Groove	0.999		0.06	< 0.001	0.998	0.002
Lat Con	0.019	0.06		0.449	0.015	0.69
Med Con	< 0.001	< 0.001	0.449		< 0.001	1
Lat Plat	1	0.998	0.015	< 0.001		< 0.001
Med Plat	< 0.001	0.002	0.69	1	< 0.001	

Table B.9: The p-values corresponding to tissue equilibrium moduli differences between sites.

	Patella	Groove	Lat Con	Med Con	Lat Plat	Med Plat
Patella		0.011	0.921	0.001	0.001	0.613
Groove	0.011		0.133	0.978	0.984	0.394
Lat Con	0.921	0.133		0.023	0.026	0.991
Med Con	0.001	0.978	0.023		1	0.102
Lat Plat	0.001	0.984	0.026	1		0.113
Med Plat	0.613	0.394	0.991	0.102	0.113	

Table B.10: The p-values corresponding to tissue dynamic moduli differences between sites.

	Patella	Groove	Lat Con	Med Con	Lat Plat	Med Plat
Patella		0.024	0.810	0.394	0.218	0.988
Groove	0.024		0.367	0.785	0.933	0.004
Lat Con	0.810	0.367		0.983	0.904	0.426
Med Con	0.394	0.785	0.983		0.999	0.125
Lat Plat	0.218	0.933	0.904	0.999		0.055
Med Plat	0.988	0.004	0.426	0.125	0.055	

Bibliography

[1] M. Heliövaara, P. Slätis and P. Paavolainen, Nivelrikon esiintyvyys ja kustannukset, *Duodecim*, 124(16):1869-74, 2008.

[2] R.F. Loeser, S.R. Goldring, C.R. Scanzello and M.B. Goldring, Osteoarthritis: a disease of the joint as an organ, *Arthritis Rheum*, 64(6):1697-707, 2012.

[3] R. Bitton, The Economic Burden of Osteoarthritis, *Am J Manag Care*, 15(8):230-5, 2009.

[4] J. Arokoski, M. Lammi, M. Hyttinen, I. Kiviranta, J. Parkkinen, J. Jurvelin, M. Tammi and H. Helminen, Nivelrikon etiopatogeneesi, *Duodecim*, 117(16):1617-26, 2001.

[5] M. B. Goldring and S. R. Goldring, Osteoarthritis, *J Cell Physiol*, 213(3):626–34, 2007.

[6] M. R. Sowers and C. A. Karvonen-Gutierrez, The evolving role of obesity in knee osteoarthritis, *Curr Opin Rheumatol*, 22(5):533–7, 2010.

[7] A. S. Anderson and R. F. Loeser, Why is osteoarthritis an age-related disease? *Best Pract Res Clin Rheumatol*, 24(1):15-26, 2010.

[8] E. Haug, O. Sand, Øysten V. Sjaastad and K. C. Toverud, Ihmisen fysiologia, WSOY, pages 232-233, 1.-3. edition, 2007.

[9] The American Academy of Orthopaedic Surgeons, OrthoInfo, http://orthoinfo.aaos.org/topic.cfm?topic=a00221, cited 25.11.2013.

[10] R. Behnke, Kinetic Anatomy, 3. Edition, p. 243-252, 2012.

[11] WebMD, http://www.webmd.com/pain-management/knee-pain/picture-of-the-knee, cited 28.11.2013.

[12] InnerBody, http://www.innerbody.com/image/skel16.html, cited 29.11.2013.

[13] S. K. Han, P. Colarusso and W. Herzog, Confocal microscopy indentation system for studying in situ chondrocyte mechanics, *Med Eng Phys*, 31(8):1038-42, 2009.

[14] A. M. Alyassin, J. L. Lancaster, J. Downs and P. T. Fox., Evaluation of new algorithms for the interactive measurement of surface area and volume, *Med Phys*, 21(6):741-52, 1994.

[15] A. D. Pearle, R. F. Warren and S. A. Rodeo, Basic Science of Articular Cartilage and Osteoarthritis, *Clin Sports Med*, 24(1):1-12, 2005.

[16] A. J. Sophia Fox, A. Bedi and S. A. Rodeo, The basic science of articular cartilage: structure, composition, and function, *Sports Health*, 1(6):461-8, 2009.

[17] J. S. Jurvelin, M. T. Nieminen, J. Töyräs, J. Risteli, M. S. Laasanen, Y. T. Konttinen and I. Kiviranta, Fysikaaliset ja kemialliset menetelmät nivelrikon varhaisessa osoittamisessa, *Duodecim*, 124(16):1885-96, 2008.

[18] A. P. Newman, Articular Cartilage Repair, *Am J Sports Med*, 26(2):309-24, 1998.

[19] Centers for disease control and prevention, http://www.cdc.gov/arthritis/data_statistics/cost.htm, cited 7.12.2013.

[20] R. Madden, S.-K. Han and W. Herzog, Chondrocyte deformation under extreme tissue strain in two regions, *J Biomech*, 46(3):554-60, 2013.

[21] I. Youn, J. B. Choi, L. Cao, L. A. Setton and F. Guilak, Zonal variations in the three-dimensional morphology of the chondron measured in situ using confocal microscopy, *Osteoarthritis Cartilage*, 14(9):889-97, 2006.

[22] B. K. Hall, Cartilage V1: Structure, Function, and Biochemistry, Academic Press, p. 322-325, 1983.

[23] K. Gelse, E. Pöschl and T. Aigner, Collagens—structure, function, and biosynthesis, *Adv Drug Deliv Rev*, 55(12):1531-46, 2003.

[24] S. M. Turunen, S.-K. Han, W. Herzog, R. K. Korhonen, Cell deformation behavior in mechanically loaded rabbit articular cartilage 4 weeks after anterior cruciate ligament transection, *Osteoarthritis Cartilage*, 21(3):505-13, 2013.

[25] F. Guilak, A. Ratcliffe and Van C. Mow, Chondrocyte deformation and local tissue strain in articular cartilage: a confocal microscopy study, *J Orthop Res*, 13(3):410-21, 1995.

[26] R. J. Wilkins, J. A. Browning and J. P. Urban, Chondrocyte regulation by mechanical load, *Biorheology*, 37(1-2):67-74, 2000.

[27] W. Stein, Transport And Diffusion Across Cell Membranes, p. 125-135, 1986.

[28] S.-K. Han, R. Seerattan and W. Herzog, Mechanical loading of in situ chondrocytes in lapine retropatellar cartilage after anterior cruciate ligament transection, *J R Soc Interface*, 7(47):895-903, 2010.

[29] P. Julkunen, W. Wilson, J. S. Jurvelin and R. K. Korhonen, Composition of the pericellular matrix modulates the deformation behaviour of chondrocytes in articular cartilage under static loading, *Med Biol Eng Comput*, 47(12):1281-90, 2009.

[30] D. J. Leong, J. A. Hardin, N. J. Cobelli and H. B. Sun, Mechanotransduction and cartilage integrity, *Ann N Y Acad Sci*, 1240:32-7, 2011.

[31] A. L. Clark, T. R. Leonard, L. D. Barclay, J. R. Matyas and W. Herzog, Heterogeneity in patellofemoral cartilage adaptation to anterior cruciate ligament transection; chondrocyte shape and deformation with compression, *Osteoarthritis Cartilage*, 14(2):120-30, 2006.

[32] P. G. Bush and A. C. Hall, The volume and morphology of chondrocytes within non-degenerate and degenerate human articular cartilage, *Osteoarthritis Cartilage*, 11(4):242-51, 2003.

[33] M. Wong, P. Wuethrich, P. Eggli and E. Hunziker, Zone-specific cell biosynthetic activity in mature bovine articular cartilage: a new method using confocal microscopic stereology and quantitative autoradiography, *J Orthop Res*, 14(3):424-32, 1996.

[34] R. K. Korhonen and W. Herzog, Depth-dependent analysis of the role of collagen fibrils, fixed charges and fluid in the pericellular matrix of articular cartilage on chondrocyte mechanics, *J Biomech*, 41(2):480-5, 2008.

[35] M. Huttu, S. Turunen, V. Sokolinski, V. Tiitu, M. Lammi and R. K. Korhonen, Effects of medium and temperature on cellular responses in the superficial zone of hypo-osmotically challenged articular cartilage, *J Funct Biomater*, 3(3):544-55, 2012.

[36] N. O. Chahine, C. Blanchette, C. B. Thomas, J. Lu, D. Haudenschild and G. G. Loots, Effect of age and cytoskeletal elements on the indentation-dependent mechanical properties of chondrocytes, *PLOS ONE*, 8(4):e61651, 2013.

[37] C. Glaser and R. Putz, Functional anatomy of articular cartilage under compressive loading Quantitative aspects of global, local and zonal reactions of the collagenous network with respect to the surface integrity, *Osteoarthritis Cartilage*, 10(2):83-99, 2002.

[38] L. Ramage, G. Nuki and D. M. Salter, Signalling cascades in mechanotransduction: cell–matrix interactions and mechanical loading, *Scand J Med Sci Sports*, 19(4):457–69, 2009.

[39] H. B. Sun, Mechanical loading, cartilage degradation, and arthritis, *Ann N Y Acad Sci*, 1211:37-50, 2010.

[40] N. P. Cohen, R.J. Foster and V.C. Mow, Composition and dynamics of articular cartilage: structure, function, and maintaining healthy state, *J Orthop Sports Phys Ther*, 28(4):203-15, 1998.

[41] J. D. Esko, K. Kimata, and U. Lindahl, Proteoglycans and Sulfated Glycosaminoglycans. In: A. Varki, R. D. Cummings and J. D. Esko, Essentials of Glycobiology, 2. edition, chapter 16, 2009.

[42] D. Eyre, Articular cartilage and changes in Arthritis: Collagen of articular cartilage, *Arthritis Res*, 4(1):30–35, 2002.

[43] R. A. Berger and A.-P. C. Weiss, Hand surgery, 1. edition, p. 5-6 2003.

[44] S.-K. Han, W. Wouters, A. Clark and W. Herzog, Mechanically induced calcium signaling in chondrocytes in situ, *J Orthop Res*, 30(3):475-81, 2012.

[45] L. G. Ameyea and M. F. Young, Animal models of osteoarthritis: lessons learned while seeking the 'Holy Grail', *Curr Opin Rheumatol*, 18(5):537-47, 2006.

[46] C. B. Little and M. M. Smith, Animal Models of Osteoarthritis, *Curr Rheumatol Reviews*, 4(3):175-82, 2008.

[47] K. D. Brandt, Animal models of osteoarthritis, *Biorheology*, 39(1-2):221-35, 2002.

[48] J. Q. Yao and B. B. Seedhom, Ultrasonic measurement of the thickness of human articular cartilage in situ, *Rheumatol*, 38(12):1269-71, 1999.

[49] J. T. Feddema and C. Q. Little, Rapid world modeling: fitting range data to geometric primitives, *Robotics and Automation*, 4:2807-12, 1997.

[50] M. J. Lammi, J. Arokoski, K. Vuolteenaho, E. Moilanen, Nivelrikon välittäjäaineet, Duodecim 2008

[51] P. Sarzi-Puttini, M. Cimmino, R. Scarpa, R. Caporali, F. Parazzini, A. Zaninelli, F. Atzeni and B. Canesi, Osteoarthritis: an overview of the disease and its treatment strategies, *Semin Arthritis Rheum*, 35(1 Suppl 1):1-10, 2005.

[52] W. C. Hayes, L. M. Keer, G. Herrmann and L. F. Mockros, A mathematical analysis for indentation tests of articular cartilage, *J Biomech*, 5(5):541–51, 1972.

[53] P. Julkunen, R. K. Korhonen, W. Herzog and J. S. Jurvelin, Uncertainties in indentation testing of articular cartilage: A fibril-reinforced poroviscoelastic study, *Med Eng Phys*, 30(4):506-15, 2008.

[54] D. J. Hunter, Y. Q. Zhang, X. Tu, M. Lavalley, J. B. Niu, S. Amin, A. Guermazi, H. Genant, D. Gale and D. T. Felson, Change in joint space width: hyaline articular cartilage loss or alteration in meniscus?, *Arthritis Rheum*, 54(8):2488-95, 2006.

[55] C. Chen, D. T. Tambe, L. Deng and L. Yang, Biomechanical properties and mechanobiology of the articular chondrocyte, *Am J Physiol Cell Physiol*, 305(12):1202-8, 2013.

[56] D. R. Keene, J. T. Oxford and N. P. Morris, Ultrastructural localization of collagen types II, IX, and XI in the growth plate of human rib and fetal bovine epiphyseal cartilage: type XI collagen is restricted to thin fibrils, *J Histochem Cytochem*, 43(10):967-79, 1995.

[57] S. Havelka, V. Horn, D. Spohrová and P. Valouch, The calcified-noncalcified cartilage interface: the tidemark, *Acta Biol Hung*, 35(2-4):271-9, 1984.

[58] F. Guilak, L. G. Alexopoulos, M. L. Upton, I. Youn, J. B. Choi, L. Cao, L. A. Setton and M. A. Haider, The pericellular matrix as a transducer of biomechanical and biochemical signals in articular cartilage, *Ann N Y Acad Sci*, 1068:498-512, 2006.

[59] D. E. Gomez, D. F. Alonso, H. Yoshiji and U. P. Thorgeirsson, Tissue inhibitors of metalloproteinases: structure, regulation and biological functions, *Eur J Cell Biol*, 74(2):111-22, 1997.

[60] Nature scitable, Microtubules and Filaments, http://www.nature.com/scitable/topicpage/microtubules-and-filaments-14052932, cited 7.5.2014.

[61] X. L. Lu and V. C. Mow, Biomechanics of articular cartilage and determination of material properties, *Med Sci Sports Exerc*, 40(2):193-9, 2008.

[62] R. K. Korhonen, M. S. Laasanen, J. Töyräs, J. Rieppo, J. Hirvonen, H. J. Helminen and J. S. Jurvelin, Comparison of the equilibrium response of articular cartilage in unconfined compression, confined compression and indentation, *J Biomech*, 35(7):903-9, 2002.

[63] M. Zhang, Y. P. Zheng and A. F. Mak, Estimating the effective Young's modulus of soft tissues from indentation tests–nonlinear finite element analysis of effects of friction and large deformation, *Med Eng Phys*, 19(6):512-7, 1997.

[64] B. V. Nguyen, Q. G. Wang, N. J. Kuiper, A. J. El Haj, C. R. Thomas and Z. Zhang, Biomechanical properties of single chondrocytes and chondrons determined by micromanipulation and finite-element modelling, *J R Soc Interface*, 7(53):1723-33, 2010.

[65] M. M. Knight, S. A. Ghori, D. A. Lee and D. L. Bader, Measurement of the deformation of isolated chondrocytes in agarose subjected to cyclic compression, *Med Eng Phys*, 20(9):684-8, 1998.

[66] E. K. Moo, Z. Abusara, N. A. Abu Osman, B. Pingguan-Murphy, W. Herzog, Dual photon excitation microscopy and image threshold segmentation in live cell imaging during compression testing, *J Biomech*, 46(12):2024-31, 2013.

[67] C. A. Poole, Review. Articular cartilage chondrons: form, function and failure, *J Anat*, 191(1):1–13, 1997.

[68] P. Tanska, S. M. Turunen, S. K. Han, P. Julkunen, W. Herzog and R. K. Korhonen, Superficial collagen fibril modulus and pericellular fixed charge density modulate chondrocyte volumetric behaviour in early osteoarthritis, *Comput Math Methods Med*, 2013, doi: 10.1155/2013/164146.

[69] K. A. Athanasiou, M. P. Rosenwasser, J. A. Buckwalter, T. I. Malinin and V. C. Mow, Interspecies comparisons of in situ intrinsic mechanical properties of distal femoral cartilage, *J Orthop Res*, 9(3):330-40, 1991.

[70] B. M. Nigg and W. Herzog, Biomechanics of the Musculo-skeletal system, John Wiley & Sons, pages 95-110, 3rd edition, 2007.

[71] V. C. Mow and C. T. Hung, Biomechanics of articular cartilage, In M. Nordin, and V. H. Frankel, Basic biomechanics of the musculoskeletal system, Lippincott Williams & Wilkins, pages 60-80, 3rd edition, 2001.

[72] John Innes Centre, `https://www.jic.ac.uk/microscopy/more/T5_8.htm`, cited 6.6.2014.

[73] R. H. Webb, Confocal optical microscopy, *Rep Prog Phys* 59:427–471, 1996.

[74] M. J. Kääb, R. G. Richards, K. Ito, I. Gwynn and H. P. Nötzli, Deformation of chondrocytes in articular cartilage under compressive load: a morphological study, *Cells Tissues Organs*, 175(3):133-9, 2003.

[75] Marvin Minsky, Memoir on Inventing the Confocal Scanning Microscope, *Scanning*, 10:128-138, 1988.

[76] J. T. Mäkelä, Z. S. Rezaeian, S. Mikkonen, R. Madden, S.-K. Han, J. S. Jurvelin, W. Herzog, R. K. Korhonen, Site-Dependent Changes in Structure and Function of Lapine Articular Cartilage 4 Weeks After Anterior Cruciate Ligament Transection, *Osteoarthritis Cartilage*, 2014, doi: 10.1016/j.joca.2014.04.010.